

# RSC Advances



This is an *Accepted Manuscript*, which has been through the Royal Society of Chemistry peer review process and has been accepted for publication.

*Accepted Manuscripts* are published online shortly after acceptance, before technical editing, formatting and proof reading. Using this free service, authors can make their results available to the community, in citable form, before we publish the edited article. This *Accepted Manuscript* will be replaced by the edited, formatted and paginated article as soon as this is available.

You can find more information about *Accepted Manuscripts* in the [Information for Authors](#).

Please note that technical editing may introduce minor changes to the text and/or graphics, which may alter content. The journal's standard [Terms & Conditions](#) and the [Ethical guidelines](#) still apply. In no event shall the Royal Society of Chemistry be held responsible for any errors or omissions in this *Accepted Manuscript* or any consequences arising from the use of any information it contains.

**Red and near infrared persistent luminescence nano-probes for bioimaging  
and targeting applications**

**S. K. Singh**

Department of Physics, Indian Institute of Technology (Banaras Hindu University), Varansi-  
21005, India

---

**Corresponding author**

*E-mail address: [sunilcfs1@gmail.com](mailto:sunilcfs1@gmail.com), [sunilks.app@itbhu.ac.in](mailto:sunilks.app@itbhu.ac.in) (S. K. Singh)*

*Tel.: +91-8574027822, Fax: +91 542 2369889*

## Abstract

The introductory aspect of the review starts with prologue on bioimaging in general and optical imaging in particular, and finally focuses onto most recently explored red and near infrared (NIR) emitting persistent luminescence nanoparticles (PLNPs) for bioimaging application. Accordingly, a prerequisite towards better understanding of the subject makes it vital to talk about persistent luminescence, and developments in red and NIR emitting persistent phosphors. In this context, different synthesis techniques to design nanoparticles and chemically-modified (surface modification) nanostructures have also been summarized. Finally, the use of these nanostructures as bioimaging and targeting probe, both for *in vitro* and *in vivo* studies, in diverse framework, has been reviewed in detail. The significant findings suggest that,  $\text{Mn}^{2+}$  and/or  $\text{Cr}^{3+}$  doped nanostructures, particularly gallogermanates, are able to give intense red-near infrared persistent emission with a longer afterglow time for more than 2 weeks and are suitable for bio-imaging applications. The review also talks about remaining challenges, new dimensions and future course of research in this field.

**Keywords:** Persistent luminescence, near infrared, gallogermanates, phosphor, bioimaging.

## 1.0 Overview

Bioimaging relates to methods that can non-invasively envisage structural and functional processes in biological materials with no/minimal affect on the life processes therein.<sup>1</sup> In recent decades, the demand for bioimaging tool has grown very rapidly, particularly for bio-medical research and medical applications. This has consequenced in the development of many advance techniques including magnetic resonance imaging (MRI), micro-computed tomography (micro CT), positron emission tomography (PET), optical coherence tomography (OCT), electrons, ultrasounds, X-ray imaging and many others.<sup>1,2</sup> These excellent bioimaging techniques cover wide observation commencing sub-cellular structures, cells, tissues up to entire multi-cellular organisms. Each technique has its own advantages and limitations too, and so more than one technique may also be used, as complementary, for complete imaging applications. However, the high cost of several of these techniques, bio-compatibility issue with tracers/markers, and a number of technological barriers impair their widespread use for routine imaging in medicals as well as for specialized research.

Optical imaging, commonly referred as fluorescence imaging also, is among one of the fastest growing field and is expected to be an alternative for other well established imaging techniques.<sup>3-21</sup> The technique basically requires luminescent bio-markers/tracers and advanced detection techniques e.g. microscopic instruments as prerequisite for most of the applications. Thus, the current research interest in this field is focused on to development of efficient optical detectors/sensors as well as to find out exotic luminescent materials as fluorescence probe. As a typical bioimaging (or biological labelling) material, fluorescent markers, such as organic dyes,<sup>3-5</sup> quantum dots (QDs),<sup>6-11</sup> plasmonic nanomaterials,<sup>12-14</sup> fluorescent proteins,<sup>15,16</sup> near infrared (NIR) fluorescent molecules,<sup>17-19</sup> *etc.* have been used successfully, but most of them usually suffer from a high photo-bleaching rate (photochemical destruction of a fluorophore under light exposure), high background light

(due to intrinsic fluorescence by bio-entities itself, e.g. body fluids and proteins are well known to give emission under UV light exposure, which results in poor signal-to-noise ratio), broad emission feature (due to molecular/band to band transition), short luminescence lifetime (typically of the order of nano/sub-micron seconds), poor biocompatibility (organic dyes and many of the QDs are readily toxic), *etc.*, which have made their use challenging until recently.<sup>20, 21</sup> In principal, these bio-markers give emission by usual fluorescence process in which high energy excitation source (e.g. UV radiation) is used to excite fluorophore, and the emission thereby is observed in visible region, which is used for visualization of different bio-entities.

Recently, colloidal solution of lanthanide doped nano-phosphors has been identified potential luminescent entities for imaging applications, as due to the unique excitation and emission features associated with them.<sup>22-27</sup> The doped lanthanide ions bear the property of frequency upconversion (UC) which allows the use of NIR (usually 980 nm) light as excitation source. Herein, UC describes a nonlinear optical process in which low energy photons are used to generate high-energy photons, usually IR radiation is used to generate visible and UV light.<sup>28-35</sup> The IR to visible UC method has been extensively applied for bioimaging application in recent decade due to their inherent merits. Remarkably, NIR light is not absorbed by biological samples, increases penetration depth in tissues, and avoids the problem of auto-fluorescence and light scattering background, *etc.*<sup>36-38</sup> The complete NIR region is considered in two main parts as far as the imaging application is concerned, i.e. NIR I (650-900 nm) and NIR II (1000-1450 nm). The choice between these two regions for imaging application is case dependent as both of them have their own features of merits. This could be understood in terms of variation in absorption and scattering by bio-entities/body fluids in these two regions. Absorption coefficient of water, haemoglobin and scattering coefficient for skin, adipose tissue and mucous tissue in NIR region have been studied well.

Fig. 1 depicts that, absorption coefficient for both haemoglobin and water is reasonably good for imaging applications. Absorption coefficient of water increases for higher wavelength side (NIR II region), but at the same time the scattering coefficient, for different types of tissues, is reduced for NIR region II.<sup>37,38</sup> Further, looking into more detail, the lanthanide ion doped inorganic nanoparticles (NPs) could maintain a photoluminescence characterized by a high photochemical stability, sharp emission bands (~10 nm, f-f transitions in lanthanide ions which remain shielded by outer s and p orbitals), long luminescence lifetimes (usually of the order of  $\mu\text{s}$  or ms), lower photo-bleaching potential, and low toxicity (LD50 value for lanthanide doped oxides is ~1000 times higher compared to QDs) as well.<sup>39</sup> However, despite their apparent advantages, such anti-Stokes probes rely strictly on higher-order coherent excitation, e.g. laser sources, which is a fundamental limitation with such materials. Lasers are costly and can excite in limited area (due to small beam diameter, typically of the order of few mm only) and at the same time NIR laser may also create heating effect (significantly temperature may rise up to the physiological order) at high input laser powers, *etc.*

Persistent luminescent materials, particularly emitting in red and NIR region, also known as long-lasting/afterglow material (both lanthanide and transition metal as active ions are known for persistent emission), could be utilized as an option to stay away from these issues with extra preferences such as nano-scale thermometry and delayed detection, and so on.<sup>40</sup> In persistent phosphors, two kinds of active centre remain involved: traps and emitters. Trap levels are originated due to lattice defects, impurities, or codopants in the material just below (sub eV to few eV) the conduction bands. On excitation with suitable energy (such as by electron beam, X rays, UV light, *etc.*), electron-hole pairs are generated and the excited electrons from the conduction band are captured in the trap levels. Traps usually do not emit radiation, but they store the excitation energy for a longer time (thus primarily act as reservoir). The process is called charging of the material. This energy can then be liberated

by thermal, optical or other physical stimulations; resulting in stimulated emissions from the active centers (process is called discharge). Thus, emitters are the centers which emit in the region of interest after getting suitable excitation energy via stimulation of the free charge from trap level (sometimes also called as persistent energy transfer process also). The key feature of such persistent phosphor is the possibility of tuning the location of the trap band (by controlling the lattice defect, doping ions, and impurity, *etc.* in the host) and thereby getting flexibility for selecting the stimulation energy source. A representative scheme to understand a general idea about different processes involved in the persistent luminescence is sketched in Fig. 2.<sup>41</sup>

The supremacy of the imaging process with such persistent luminescence materials could be acknowledged with three distinctive features.<sup>41</sup> The first and the most paramount one is the persistent luminescence itself: intense, long-lasting persistent light (up to several hundred hours) emanating by the material extensively much after the removal of the excitation (usually UV, X-rays, electron beam, *etc.*) source. This allows imaging without external excitation, which completely removes the likelihood of auto-fluorescence/background noise and thus a significant improvement in signal-to-noise ratio and sensitivity is attained. Secondly, the emission in red-NIR region (particularly in 650-1000 nm range) lies in the tissue transparency window,<sup>42,43</sup> in which light attenuation is largely due to scattering rather than absorption which further increases the detection depth. The third one is the possibility of photo-stimulation, to rejuvenate the persistent luminescence after long period, through incoherent light source, e.g. by light emitting diodes (LEDs)/flash lamps, and even by Sun light *etc.*, which makes the long time imaging effective, easier, cost effective and safe. Recently, in last few years, this imaging technique has been quite popular and a significant progress has been achieved in such a short span of time and still great efforts are in progress. Nevertheless, a review on this subject is still not available. A brief review on the

NIR persistent luminescence based nanostructures with a special reference to bioimaging thereof may be quite useful not only to follow the new progress in this field, but also to construct and design new probes for imaging applications.

This review is an attempt to present an overview of the persistent luminescence, particularly covering red and NIR persistent material, and their application for bioimaging. The main focus is on NIR persistent luminescence in transition metal (Mn and Cr) doped nano-structures. Different synthesis techniques to design nanocrystalline particle and chemically-modified (surface modification) nanostructures of such materials for imaging purposes are summarized. A detail of the structure, effect of doping of different ions on the structure, origin of defect levels (trap levels) and different mechanisms to tune the depth of the trap levels in such materials has also been included in the study so as to build up an understanding of the persistent luminescence. Further, in continuation, different optical parameters e.g. thermal stimulation, photo-stimulation by coherent/incoherent/Sunlight sources, persistent energy transfer from trap level to the active ion, persistent luminescence stability and reproducibility, effect of power/temperature/charging time *etc.* on the persistent luminescence have also been considered. Finally, the use of this material as bioimaging probe, both for *in-vitro* and *in vivo* studies in different system, along with the acute and chronic toxicity studies have been reviewed in detail. In the final remarks, the review talks about the remaining challenges, and future direction of the research in this field.

## 2.0 Persistent luminescence

A pre-requisite towards better understanding of the subject makes it essential to discuss persistent luminescence, its development, present status of the field, literary review of the existing persistent phosphors, *etc.* Persistent luminescence is a phenomenon whereby luminescence can last for hours (or even more, recently reported upto few days) after the stoppage of the excitation.<sup>44-53</sup> As mentioned earlier, it is generally accepted that, the presence

of lattice defects causes the evolution of trap levels which play central role for afterglow/persistent luminescence in some potentially efficient luminescent materials. But, even after a long history of work on persistent luminescence, the fundamental of each and every steps involved in this phenomenon is still not unanimously accepted, more than one explanation are available in published articles to explain certain process. The review article by Brito *et. al.* focuses on to the mechanisms of persistent luminescence. Not only the mechanism, but this interesting article also comments on diverse names that are utilized for persistent luminescence.<sup>46</sup> The article remarks that, some of the names are used as adjectives e.g. long, persistent, long-duration and long-lasting while few others as nouns e.g. afterglow, fluorescence, phosphorescence and luminescence. Not just this, names have likewise been utilized even as a part of sets of two, or in still greater gatherings additionally e.g. long-persistent phosphorescence, *etc.*<sup>46</sup> However, persistent luminescence is alluded to a special case of thermally stimulated luminescence at a given temperature (usually at room temperature), which ought to be different from phosphorescence due to forbidden transition in the luminescence center.

Persistent luminescence was at first not all that appealing for researchers working in the area of luminescent materials. Therefore, else, it was viewed as the undesired property for the luminescent materials, as the presence of lattice defects usually quenches the luminescence property considerably, and its utilization was likewise exceptionally constrained. Some typical sulfide based materials with a persistent luminescence time on the order of few hours with weak intensity were in use, but at the cost of potential risk of environmental hazards.<sup>46,47</sup> Application of lanthanide ions for persistent luminescence revolutionized this field. In last few years, at this point, more than 200 combinations of host materials and activator ions have been depicted, of which around 20% or thereabouts are singularly focused around divalent europium ( $\text{Eu}^{2+}$ ) and co-dopant ions.<sup>44</sup> Generally, most of the lanthanide ions have been used

to get persistent luminescence, essentially in different colours. Recently, Tadashi *et. al.* explored persistent luminescence of most of the lanthanide ions in  $\text{Ca}_2\text{SnO}_4$  host.<sup>45</sup> Fig. 3 gives a beautiful digital photograph of the emission and afterglow both by different lanthanide ions. A large number of potential applications of the persistent luminescence e.g. traffic signs, emergency signage, watches, clocks, textile printing, forensic applications: security ink, latent fingerprint detection, photovoltaic application: to increase the conversion efficiency of silicon solar cells, and certainly for bioimaging/tagging, *etc.* have been successfully demonstrated and few of them have been commercialized also, till date.<sup>48-53</sup> The use of lanthanide ions for persistent luminescence is considered among one of the latest applications of lanthanide ions following its application for lasers, fibres, IR to visible frequency UC, advance lighting and display devices, imaging, *etc.*<sup>54,55</sup>

The original concept for the development of lanthanide doped persistent luminescent material was centred on  $\text{Eu}^{2+}$  ions in different host matrices including glass (silicate and borate), ceramics (aluminates, aluminosilicates), *etc.* The  $\text{Eu}^{2+}$  doped alkaline earth (Ca, Sr) aluminates remain, however, most important persistent phosphors, especially because the afterglow is greatly enhanced by co-doping with some trivalent lanthanide ions, particularly  $\text{Dy}^{3+}$  and  $\text{Nd}^{3+}$  ions.<sup>56</sup> It was proposed that in such phosphors, reduction of  $\text{Eu}^{2+}$  to  $\text{Eu}^{3+}$  and oxidation of  $\text{Nd}^{3+}/\text{Dy}^{3+}$  to  $\text{Nd}^{4+}/\text{Dy}^{4+}$  occurs in the persistent luminescence processes, which was not completely acceptable due to many reasons.<sup>57-59</sup> But, among them,  $\text{CaAl}_2\text{O}_4:\text{Eu}^{2+}$ ,  $\text{Nd}^{3+}$  and  $\text{SrAl}_2\text{O}_4:\text{Eu}^{2+}$ ,  $\text{Dy}^{3+}$  have already been in use commercially for many of the applications listed above. The group of Smet summarizes origin, development and advancement in the field of lanthanide doped persistent luminescence phosphor for all the blue, red, green and white light colours in two review articles.<sup>40,60</sup>

In addition to this, a recent review by Tanabe group gives a short description about red and NIR emitting phosphors which is planned basically to emphasize state-of-the-art

development of such persistent phosphor only.<sup>61</sup> The review comments on to the evaluation method of red to NIR persistent luminescence intensity. They summarize that, the generally adopted evaluation method for persistent phosphors is *luminance* (in units of  $\text{cd m}^{-2}$ ) which is not suitable for red to NIR persistent phosphors particularly aiming to the application of *in vivo* imaging. Instead, the use of *radiance* (in units of  $\text{W sr}^{-1} \text{m}^{-2}$ ), which is not related to the human eye sensitivity, is more suitable and can be adopted. Further, the review lists a brief detail of the host and activator ions for red-NIR emission and mechanism involved in persistent luminescence; however, it completely overlooks the bioimaging part which is the major attraction of research and development for NIR persistent phosphors now a days.

### 3.0 Red emitting persistent material and bioimaging application

After making initial introduction and background of the subject in first two sections, this section put forwards a proper focus on red emitting persistent material and their biological applications. Initially, most of the red emitting afterglow phosphors were sulphide based lanthanide doped phosphor. CaS, SrS, BaS or their combination e.g.  $\text{Ca}_{1-x}\text{Sr}_x\text{S}$  doped with different combination of dopants.<sup>62-74</sup> Most of these sulphide based phosphors contain  $\text{Eu}^{2+}$  as one activator ion along with other co-dopants such as  $\text{Tm}^{3+}$ ,  $\text{Dy}^{3+}$ ,  $\text{Ce}^{3+}$ ,  $\text{Pr}^{3+}$ ,  $\text{Bi}^{3+}$ , *etc.* In addition to this, effect of alkali ions (e.g. co-doping of  $\text{Li}^+$ ,  $\text{Na}^+$ ), halides (Cl) *etc.* on luminescence/persistent luminescence have also been done. A review article by Ghosh *et. al.* throws light over the developments of alkaline earth sulphides (e.g. CaS, SrS and BaS) as luminescent and energy storage materials.<sup>62</sup> This includes developments about brief understanding of the subjects, particularly defect states in these sulphides attained through studies of electron spin resonance (ESR), thermally stimulated luminescence (TSL) and fluorescence emission spectra at low and elevated temperatures. This review article also covers evolution of new preparation methods for polycrystalline powders, thin film layers and single crystals, *etc.* In one of the recent works on sulphide phosphor, Burbano *et. al.*

have developed NPs of CaS codoped with  $\text{Eu}^{2+}$  and  $\text{Dy}^{3+}$ , having particle size nearly 80 nm, and realized efficient red persistent luminescence by photo-stimulation (through 900 nm, 950 nm and 980 nm IR laser) and have suggested its potential application for optical information storage. Storage of energy by UV excitation can serve as the writing process and release of the stored energy by photo-stimulation through near IR light excitation can serve as the reading process.<sup>74</sup>

The CaS and SrS are the phosphors which have a great variety of emission centre and perform a wide range of colours. But, such phosphors are extremely sensitive to moisture and thus chemically unstable. To make them stable, surface modification becomes essential. Further to remove this lacuna, oxysulfide phosphors were tried and developed at the next step.<sup>75-80</sup> In this line,  $\text{Y}_2\text{O}_2\text{S}:\text{Eu}^{3+}$  is very well known as afterglow phosphor emitting in orange-red region, near at 621 nm. Other co-dopant such as Ti and Mg are also used basically to control the defect/trapping centres.  $\text{Sm}^{3+}$  has also been used as an activator to get orange-red emission in oxi-sulphide hosts. Several other phosphors in different hosts e.g. silicates,<sup>81-90</sup> germanate,<sup>91,92</sup> nitride,<sup>93</sup> stannate,<sup>94</sup> phosphates,<sup>95-102</sup> aluminates,<sup>103</sup> titanate,<sup>104,105</sup> metal oxides,<sup>106,107</sup> fluorides,<sup>108</sup> and others,<sup>109</sup> have also been developed for getting long afterglow emission in red region. Table 1 gives a comprehensive detail of the host, dopant ions, colour/wavelength of the afterglow emission, persistent time, and remarks, if any of the red emitting persistent phosphor.<sup>64-109</sup>

The work by Lecoindre *et. al.* presents a new concept to design red persistent phosphor in yttrium phosphates.<sup>99</sup> They codoped the material with  $\text{Ce}^{3+}$ ,  $\text{Ln}^{3+}$  and  $\text{Pr}^{3+}$ ,  $\text{Ln}^{3+}$  (Ln = Nd, Er, Ho and Dy) to realize the red persistent luminescence. The study was explored on the basis of TSL measurement and it was found that similar to  $\text{Ce}^{3+}$ ,  $\text{Pr}^{3+}$  was also able to trap holes up to high temperatures while being the radiative recombination center, whereas, the  $\text{Ln}^{3+}$  codopants played the role of the electron trap. In a similar work, Bessiere *et. al.*

proposed  $\text{Ca}_3(\text{PO}_4)_2$ , a highly biocompatible compound, for colour tunable red long lasting luminescence.<sup>101</sup>  $\text{Mn}^{2+}$  was selected as dopant to serve as the active luminescent centre displaying its  ${}^4\text{T}_1$  ( ${}^4\text{G}$ )/ ${}^6\text{A}_1$  ( ${}^6\text{S}$ ) broad emission at 660 nm and substituting the small octahedral Ca site of the host. Further, codoping with trivalent lanthanide ions ( $\text{Dy}^{3+}$ ,  $\text{Tb}^{3+}$ ) enhances the  $\text{Mn}^{2+}$  optical luminescence (X-ray excited), while on the other hand, delayed luminescence originating from carrier trapping is suppressed.  $\text{Ca}_3(\text{PO}_4)_2:\text{Mn}^{2+}$ ,  $\text{Dy}^{3+}$  showed the most intense long lasting luminescence. Lian *et. al.* developed a Ca and Zn based titanate phosphor and realized dual persistence luminescence originated at 614 and 644 nm induced by two separate kinds of doping defects. Further they suggests the application of this material in energy conversion.<sup>105</sup>

All the listed compositions of red phosphors in table 1 were prepared basically to realize the red-persistent luminescence, however, there was very few specific application for persistent luminescence based bioimaging. In this context, Maldiney *et. al.* synthesized  $\text{Ca}_2\text{Si}_5\text{N}_8$  (CSN) simply by mixing the stoichiometric amounts of required compounds and then sintered the material at 1300 °C under reducing atmosphere (90%  $\text{N}_2$ , 10%  $\text{H}_2$ ).<sup>109</sup> Further, the powder material (pressed to form a small target of the diameter of 8 mm) was subjected to pulsed laser ablation technique to extract NPs in solution. Significantly, small NPs with diameters in the range of 3-5 nm were obtained, but the low quantity in solution prevents further use of the material for bioimaging. However, further they used wet grinding technique to extract NPs which gives enough NPs to realise the use of this material as optical probe for small animal *in vivo* imaging. This technique successfully translates the present bulk nitridosilicate powder to obtain a narrow size distribution of negatively charged hydroxyl-terminated CSN NPs with a mean diameter close to 200 nm; however, the yield is 10% only. Surface functionalization of the NPs were done by using poly-ethylene glycol

(PEG) grafting so as to get better distribution of the NPs after systemic injection, delaying their uptake by the reticulo-endothelial system (RES).

Expect such few rare examples; it was hard to find bioimaging application by red emitting persistent phosphor. Indeed, few of them, particularly emitting in red region ( $\geq 650$  nm) could be used for imaging application in principle. Nevertheless, most of the developed phosphor has been synthesized involving high temperature synthesis technique, e.g. solid state reaction method or by high temperature solution combustion synthesis followed by high temperature post-annealing, which ultimately results the development of particle size in sub-micron to micron range, not usable for bioimaging applications. Thus, new synthesis strategies for evolution of ultrafine particles, effective surface functionalization strategies along with the bio-compatibility issues need more attention to make them useful for bioimaging applications further.

#### **4.0 Near infrared emitting persistent nanostructures and bioimaging application**

Bioimaging, undoubtedly, is best performed with red-NIR radiation (both as excitation and/or emission); the reasons behind have already been discussed in previous sections. Even though, it is worthwhile here to mention that, probe detection is governed mainly by emission intensity of the luminescent probe, optical path length through tissue and volumetric energy distribution; all of these are significantly concurrent to absorption and scattering properties of biological media and tissues.<sup>110</sup> For a ready reference, the most favourable window for arteries is considered between 634 nm and 756 nm with the minimal absorption coefficient at 686 nm, while for veins the optimal NIR window lies between 664 nm to 932 nm with the minimal absorption coefficient at about 730 nm for imaging applications.<sup>111</sup>

A wide variety of luminescence centres have been developed and used as NIR luminescent probes for imaging applications. Recently, a review by Wang *et. al.* gives a comprehensive detail of different types of nanomaterials that can be excited/can emit in NIR I

(650-900 nm) and NIR II (1000-1450 nm) regions.<sup>112</sup> Wide ranges of materials have been reviewed e.g. lanthanide based NPs (both UC and downconversion based), carbon based nanostructures (e.g. carbon dots, carbon nanotubes, graphene, *etc.*), quantum dots (e.g. CdS, CdTe, CdSe, ZnSe, InAs, PbS, Ag<sub>2</sub>S, *etc.*) and noble metal nanomaterials (silver and gold metal nanoclusters), *etc.* for fabrication and application in bioimaging. The review, of course, put forwards shortcomings, challenges and opportunities associated with them also. But, when it comes to NIR persistent luminescence based materials; such comprehensive article is very rare or completely missing. This is due to the fact that, numbers of known activators for NIR persistent luminescence are relatively low and less explored. Contrary to wide availability of research articles related to IR emission in lanthanide doped material, only few works related to lanthanide doped (only) materials possessing NIR persistent luminescence is reported so far. The majority of research for NIR persistent luminescence is based on transition metals, mainly either based on Mn<sup>2+</sup> and/or on Cr<sup>3+</sup> as one of the dopant ion. Besides these two main classes of activators, scarcely any other ions have been found to exhibit persistent luminescence in NIR region particularly of the interest of bioimaging application. Therefore, available articles/materials based on these activators are further reviewed into three different subsections as follows.

#### **4.1 Lanthanide (only) doped persistent materials and bioimaging**

Lanthanides are well known for their ladder like dense energy level structures through which they can generate emission ranging from UV-visible to NIR regions. However, in a more specific sense, lanthanide NIR-emitting ions are usually limited to those ions which mainly emit prominently in NIR spectral regime (700-2500 nm). Recent articles by Bunzali and his group summarizes the most important NIR-emitting Ln(III) ions and their characteristic transitions in NIR region.<sup>113,114</sup> The main lanthanides described are Pr, Nd, Sm, Dy, Ho, Er, Tm and Yb which gives prominent NIR emission. But, when it comes to NIR persistent

emission, most of the lanthanide ions, capable of generating NIR emissions, cannot be adopted. This is mainly due to the fact that, the 5d state of lanthanides is too high to charge, and in addition to this, they usually possess prominent visible emissions in addition. Thus, the key barrier that limits the development of NIR persistent phosphors using lanthanide ions is the lack of carrier traps with suitable thermal release rate at room temperature. Recently, a concept of persistent energy transfer (PET) between two different emitting centres has been proposed to direct the design of visible/NIR persistent phosphors. In this concept, persistent emission at shorter wavelength (say, UV/visible) by entity 1 is absorbed by entity 2 which latter on may emit persistently at longer wavelength (say, visible/NIR). Very few research articles are available which reports NIR persistent luminescence from lanthanide ions, and if available, most of them are based on PET among different lanthanide ions.<sup>115-117</sup> However, bioimaging from any such NIR persistent phosphor is rarely reported.

Recently, Jumpei *et al.* reported NIR persistent luminescence due to  $\text{Nd}^{3+}$  ( ${}^4\text{F}_{3/2} \rightarrow {}^4\text{I}_{1/2}$ ) ion in the  $\text{CaAl}_2\text{O}_4$  host co-doped with  $\text{Eu}^{2+}$  ion.<sup>115</sup> They prepared samples with compositions  $\text{Ca}_{0.995}\text{Eu}_{0.005}\text{Al}_2\text{O}_4$ ,  $\text{Ca}_{0.99}\text{Nd}_{0.01}\text{Al}_2\text{O}_4$  and  $\text{Ca}_{0.985}\text{Eu}_{0.005}\text{Nd}_{0.01}\text{Al}_2\text{O}_4$  by conventional solid state reaction method and further studied optical properties e.g. reflectance, photoluminescence, persistent luminescence and afterglow decay curves, *etc.* The decay curves for the persistent luminescence of  $\text{Eu}^{2+}$  and  $\text{Nd}^{3+}$ , after 10 min of excitation by UV (330 nm) light, is shown in Fig. 4(a). The decay profiles of  $\text{Eu}^{2+}$  and  $\text{Nd}^{3+}$  are quite similar. Authors explain the persistent luminescence in terms of energy transfer from  $\text{Eu}^{2+}$  to  $\text{Nd}^{3+}$  ions.  $\text{Eu}^{2+}$  ion is photo-oxidized into  $\text{Eu}^{3+}$  or  $(\text{Eu}^{2+} + \text{h}^+)$  and the electron can be trapped by some defects derived from  $\text{Nd}^{3+}$  codoping. Process of de-trapping takes place via heat and recombination with the photo-oxidized  $\text{Eu}^{3+}$  ions. The persistent luminescence intensity ratio for  $\text{Nd}^{3+}$  to  $\text{Eu}^{2+}$  remains almost constant with a variation in time. This concludes that, persistent luminescence from both the ions originates from a common electron trap and

electron transfer process. Further, this also support for an energy transfer from  $\text{Eu}^{3+}$  to  $\text{Nd}^{3+}$ . Tang *et. al.* have also reported NIR persistent emission of  $\text{Nd}^{3+}$  ion in strontium aluminate host.<sup>116</sup>

Another example of NIR persistent luminescence in lanthanide,  $\text{Er}^{3+}$ , has been reported by Yu *et. al.* in  $\text{SrAl}_2\text{O}_4$  host codoped with  $\text{Eu}^{2+}$  and  $\text{Dy}^{3+}$  ions.<sup>117</sup> Detailed structural, excitation, emission and decay time characteristics have been explored. Herein, again an energy transfer mechanism has been identified behind the persistent NIR emission. The phosphors were synthesized through the combustion method with composition  $\text{SrAl}_2\text{O}_4:1\% \text{Eu}^{2+}, 1.5\% \text{Dy}^{3+}, x\% \text{Er}^{3+}$ , where  $x=0.5-2.5$ , particle size of the phosphor lies in the range of 17-27 nm. Excitation spectrum depicts that, the peak at 518 nm arising due to  $^4\text{I}_{15/2} \rightarrow ^2\text{H}_{11/2}$  transitions of  $\text{Er}^{3+}$  ions totally overlaps with the 525 nm green emission bands of the  $\text{Eu}^{2+}$  ions which suggest for a fair possibility of an efficient energy transfer from  $\text{Eu}^{2+}$  ions to  $\text{Er}^{3+}$  ions. Fig. 4(b) shows the afterglow decay curves of  $\text{SrAl}_2\text{O}_4: 1.0\% \text{Eu}^{2+}, 1.5\% \text{Dy}^{3+}$ , and 2%  $\text{Er}^{3+}$  phosphor for 525 nm green emission and 1530 nm NIR emission. The charge trapping and ET process is shown in the inset to Fig. 4(b). In comparison to green afterglow (more than 10 h), NIR decay time is much shorter (only about 10 minutes). This big difference in afterglow time is because of the fact that,  $\text{Er}^{3+}$  ions not only act as efficient NIR emitters but also function as effective charge trap centre. Authors have discussed in detail the different processes involved in trapping and de-trapping. Except these few specific examples, it is hard enough to find lanthanide based NIR persistent phosphor. Thus, it is summarized that, although lanthanide doped NIR persistent luminescent materials are available, yet, they are very small in number and at the same time the persistent time is quite low (upto few minutes only) which limits their applications in bioimaging.

#### 4.2 $\text{Mn}^{2+}$ doped persistent materials and bioimaging

$\text{Mn}^{2+}$  possesses an incompletely filled d shell and its electronic configuration is  $d^5$  (transition metals are most stable when their d orbitals have either 5 or 10 electrons, so Mn loses the 4s electrons first to structure  $\text{Mn}^{2+}$ ). Since the energy levels lie within the d shell, all transitions from the ground state to excited levels are spin and parity forbidden. Nevertheless, the selection rule is relaxed a little bit through a spin-spin interaction and a vibronic mechanism, where the electronic transitions are coupled with vibrations of suitable symmetry.<sup>118-122</sup> Due to the involvement of outermost d shells, unlike the lanthanide ions where inner f-f transitions are involved, the transitions from transition metal ions, e.g.  $\text{Mn}^{2+}$ , are affected considerably by crystal/ligand field. The interaction between a central metal ion surrounded by anions in different possible geometry (namely spherical, linear, square planar, tetrahedral, or octahedral) is portrayed utilizing Crystal Field Theory (CFT). Complete spherical symmetry is not observed in real aspects usually. The geometry of the negatively charged point charges influences the energy level of the central metal ion. In case of transition metal like  $\text{Mn}^{2+}$  and  $\text{Cr}^{3+}$ , 3d orbital being the outermost shell is affected most. Specific geometry due to point charges produces a characteristic splitting pattern. The extent of the splitting in energies is represented by the splitting energy  $\Delta$ . A subscript is used further to specify the geometry of the surrounding point charges, for example *t* for tetrahedral and *o* for octahedral, *etc.*

Tanabe and Sugano have estimated the energy levels of  $\text{Mn}^{2+}$  by considering the interaction between the d electrons and different types of the point charge/crystal field environment, e. g. linear, square planar, tetrahedral and octahedral.<sup>118-120</sup> The energy levels of a free Mn ion includes the terms  $^6\text{S}$ ,  $^4\text{G}$ ,  $^4\text{D}$ ,  $^4\text{P}$ ,  $^4\text{F}$ ..., *etc.* The levels of the free ions are manifested as  $^{2S+1}\text{L}$ , where S presents the total spin quantum number, and L is the total orbital angular momentum. Many of these levels split into two or more levels and the degeneracy of these levels is given by  $2L+1$ . These crystal fields modified degenerate energy levels are represented by  $^{2S+1}\text{X}$ , where X usually correspond to A for no degeneracy, E for a two-fold

degeneracy and T for a three-fold degeneracy. The red/NIR emission in  $\text{Mn}^{2+}$  is observed due to the lowest energy multiplet of first excited state  ${}^4\text{T}_1$  (G) to the ground state  ${}^6\text{A}_1$  (S). Usually red persistent emission is observed in most of the host by  $\text{Mn}^{2+}$  ions (refer table 1), while NIR persistent luminescence has been realized in few hosts only. Table 2 gives a comprehensive detail of the host, dopant ions, wavelength of the afterglow emission, and remarks, if any of the NIR emitting persistent phosphor activated with  $\text{Mn}^{2+}$  ion.<sup>40, 123-129</sup>

The credit for the first use of  $\text{Mn}^{2+}$  doped persistent nanophosphor for *in vivo* imaging application goes to the group of Daniel Scherman.<sup>40</sup> The material was co-doped with lanthanide ions ( $\text{Eu}^{2+}$  and  $\text{Dy}^{3+}$ ). The group selected  $\text{MgSiO}_3$  host for the purpose, which was already reported for red persistent luminescence arising due to  $\text{Mn}^{2+}$ .<sup>81</sup> The group did two new things; first they altered composition of the host lattice, by introducing Ca and Zn, to optimize the emission of  $\text{Mn}^{2+}$  in IR region. Secondly, they synthesized this phosphor ( $\text{Ca}_{0.2}\text{Zn}_{0.9}\text{Mg}_{0.9}\text{Si}_2\text{O}_6$ ) via sol-gel synthesis technique followed by selective sedimentation process so as to reduce the particle size usable for imaging applications. By this way, they were able to get particles with diameter ranging from 50 to 100 nm. The X-ray diffraction (XRD) pattern and transmission electron microscopy (TEM) image of the sample is shown in Fig. 5(a) and Fig. 5(b), respectively.

Authors explain persistent luminescence as due to  $\text{Mn}^{2+}$  (activator ion). Trap centres are created due to  $\text{Dy}^{3+}$  doping and lanthanide ions act as primary acceptor of energy, which is thermally released to  $\text{Mn}^{2+}$  ions (through tunnelling and PET processes). The change in composition changes symmetry and crystal field strength at  $\text{Mn}^{2+}$  site which is responsible for emission from red to NIR corresponding to well known  ${}^4\text{T}_1(4\text{G})$  excited state to the  ${}^6\text{A}_1(6\text{S})$  fundamental state. The excitation (for  $\lambda_{\text{exc}}=690$  nm) and emission (for  $\lambda_{\text{ems}}=340$  nm) spectrum are shown in Fig. 5(c) and Fig. 5(d), respectively. The broad nature of the excitation band also support for an energy transfer process, as this could not be solely due to the transitions of

Mn<sup>2+</sup> ion. The decay curve of luminous intensity shows that the persistent luminescence is detectable for about 24 h, when kept in the dark. The decay kinetics (shown in Fig. 5(e)) were found to be close to a power law  $I \approx I_0 x t^{-n}$  ( $n=0.96$ ,  $R^2=0.996$ ) after the first 100 s.

In the next step, the persistent NPs were surface functionalized to make them amiable for imaging application. Three different surface modifications namely amino, carboxyl and PEG were tried. Amino-NPs were synthesized by reaction with 3-aminopropyltriethoxysilane, carboxyl-NPs were obtained from a reaction of amino-NPs with diglycolic anhydride, and PEG-NPs were achieved by a peptidic coupling of amino-NPs with PEG5000COOH. Schematic representation of surface modification of NPs through different capping agents is shown in Fig. 5(f). These surface functionalized particles were developed with different surface charge. Authors have shown different aspects of imaging with these surface modified NPs. In the first step, simple visualization of persistent luminescence in mice is observed after subcutaneous (SC) and intramuscular (IM) injection of the NPs. The lowest dose administered, even 20 ng, produces a detectable signal with a satisfactory signal-to-noise ratio superior to 5 during SC injection; while a comparatively higher dose, 20  $\mu$ l at 10 mg/ml, is required for satisfactory result during IM injection. In the second step, optical imaging of mouse with 1 mg tail vein injections of differently charged NPs were carried out. Fig. 5(g) shows imaging with amino-NPs. Results depict that, bio-distribution of NPs depends on the surface charge, differently charged NPs possess markedly altered bio-distribution. Furthermore, the use of anionic liposomes before NP injection has been found to be a powerful method to improve targeting to specific organs, and PEG-NPs (after preinjection of anionic liposomes) have been used to visualize tumour in mouse successfully.

In the continuation of their work towards the enhancement of imaging process in many aspects, further, in their next work, the group modified the surface coating of the persistent NPs with methoxy-PEG of varying molecular weight (5, 10, and 20 kDa) and also varied the

particle size of the persistent phosphor.<sup>123</sup> Earlier used PEG-NPs were mainly absorbed by RES organs, mostly liver and spleen. Nevertheless, use of methoxy-PEG extends persistent luminescence nanoparticles (PLNP) circulation in mice and concludes that, blood retention capability of PLNPs is highly dependent on the particle core diameter as well as on surface coating. However, they further point out that, increasing molecular weight of the PEG moiety, from 5 to 20 kDa, had no significant effect on combined uptakes in major RES organs such as liver and spleen. Small and stealth PEGylated PLNPs were shown to circulate for much longer period, postponing the uptake from the RES organ only, which shows its promise for future application in targeting and cancer imaging.<sup>123</sup>

In another novel application of the same PLNPs, the group successfully reported the first use of biotinylated PLNPs to target avidin-expressing glioma cells.<sup>124</sup> In this process, PEGylated PLNPs were functionalized by biotin to form biotin-PEG-PLNPs and further the system was used to target biotin-binding proteins e.g. streptavidin and neutravidin. Firstly, biotinylated PLNPs are allowed to bind with streptavidin coated on a plate. It is marked that, the presence of a PEG spacer is critical to allow the efficient binding to streptavidin coated on a plate. Secondly, interaction with free neutravidin in solution was confirmed by fluorescence microscopy. Finally, *in vitro* binding study on BT4C cells expressing lodavin fusion protein, bearing the extracellular avidin moiety, is done and has been used to target the malignant glioma cells through a specific biotin-avidin interaction. In a similar work for targeting strategies, the group reports design and functionalization of PLNPs with small targeting molecules.<sup>125</sup> The first example they take is the functionalization of PLNPs with biotin in order to evaluate their binding affinity on streptavidin coated plate, which is somewhat explained in their earlier work too.<sup>124</sup> The second and novel example they target is the functionalization of PLNPs with Rak-2 molecule, a well known molecule for its affinity toward PC-3 cells. The Rak-2 functionalized PLNPs show high stability in complete DMEM

(Dubecco's modified Eagle's medium) culture medium and preliminary results reported by the group depicts immobilization of PLNP-PEG-biotin on streptavidin plate and binding of PLNP-PEG-Rak-2 on prostate cancer cells.

Thus in this way, the group exploited few important bioimaging applications (both *in vivo* and *in vitro*) of the  $\text{Mn}^{2+}$  doped persistent phosphor, but at the same time, they realized that improvement in the persistent emission intensity/persistent time is essential for long-term monitoring of *in vivo* probe accumulation which needs more work towards the development of new PLNPs with improved optical characteristics. Authors came up with a new idea that, controlling electrons trap depth could help to enhance the optical properties of PLNPs. In this context, they synthesized several  $\text{Mn}^{2+}$  doped diopside NPs, either codoped with trivalent lanthanide ions, e.g.  $\text{CaMgSi}_2\text{O}_6:\text{Mn}^{2+}, \text{Ln}^{3+}$  ( $\text{Ln} = \text{Dy}, \text{Pr}, \text{Ce}, \text{Nd}$ ) abbreviated as CMSO:Ln, which can be excited with X-rays only, or tridoped with divalent europium and trivalent lanthanide ions, e.g.  $\text{CaMgSi}_2\text{O}_6:\text{Mn}^{2+}, \text{Eu}^{2+}, \text{Ln}^{3+}$ , to enable UV excitation, abbreviated as CMSO.<sup>126</sup> The main aim was to tune the trap depth by co-doping with  $\text{Ln}^{3+}$  ion and to find a particular lanthanide ion for optimized IR emission suitable for bioimaging application. Schematic energy level diagram of  $\text{Mn}^{2+}$  and  $\text{Ln}^{3+}$  in CMSO is shown in Fig. 6(a). The relative positions of electron trap levels originating due to different lanthanide ion co-doping with respect to the conduction band edge is expanded as shown in the inset of the energy level diagram in Fig. 6(a). Trap depth due to Pr, lying below to  $\text{Ce}^{3+}$  and above to  $\text{Nd}^{3+}$ , has been identified as the optimal electron trap in the diopside host, which led to an improved nanomaterial, excitable with UV light and displaying the most intense afterglow in the NIR region. Further, they used the novel and optimized composition ( $\text{CaMgSi}_2\text{O}_6:\text{Eu}^{2+}, \text{Mn}^{2+}, \text{Pr}^{3+}$ ) for *in vivo* imaging via intravenous injection of such PLNPs in mice for sensitive detection through living tissues. They also compared this material with earlier reported phosphor composition abbreviated here as CZMSO, i.e.  $\text{Ca}_{0.2}\text{Zn}_{0.9}\text{Mg}_{0.9}\text{Si}_2\text{O}_6$  co-doped with

Eu<sup>2+</sup>, Dy<sup>3+</sup>, Mn<sup>2+</sup>, during imaging application, shown in Fig. 6(b, c), respectively. They report improved imaging with CaMgSi<sub>2</sub>O<sub>6</sub>:Eu<sup>2+</sup>, Mn<sup>2+</sup>, Pr<sup>3+</sup> composition.

In a similar work, Li *et. al.* have synthesized SiO<sub>2</sub>/CaMgSi<sub>2</sub>O<sub>6</sub>:Eu<sub>0.01</sub>, Pr<sub>0.02</sub>, Mn<sub>0.10</sub> persistent phosphor emitting with its persistent emission maximum at 660 nm.<sup>127</sup> The article covers synthesis and characterization (structural-phase, morphology, optical) of the NPs, surface functionalization, cell viability (through cytotoxicity) test, and *in vivo* imaging (on mouse). NPs have been obtained with control over morphology and size. Hydrophilic modification has been carried out further, which shows that nanoprobe exhibit good biocompatibility. The cell viability test shows that, NPs are metabolized from the lymph circulation and transferred from abdomen to bladder. The afterglow emission of the as-prepared nano-probes successfully used to track the real time bio-distribution *in vivo* with reasonably good signal-to-noise ratio.

Different from silicate host, Pang *et. al.* recently reported NIR persistent emission due to Mn<sup>2+</sup> ions in zinc pyrophosphate, Zn<sub>2(0.97-x)</sub>P<sub>2</sub>O<sub>7</sub>:0.06Tm<sup>3+</sup>, 2xMn<sup>2+</sup> (0 ≤ x ≤ 0.05), host.<sup>128</sup> A series of new phosphors were synthesized by using the typical high temperature solid-state reaction method. Both single doped and co-doped samples crystallize into mono phase, α-Zn<sub>2</sub>P<sub>2</sub>O<sub>7</sub>. The doping of Mn<sup>2+</sup> and/or Tm<sup>3+</sup> do not alter the phase, only a slight variation of the cell volume is seen, this may be due to the differences of ionic radius and valence between Zn<sup>2+</sup> and the doping ions (Mn<sup>2+</sup>, Tm<sup>3+</sup>), which confirms the substitution by the doping ions into the host lattice. Further detailed photoluminescence, persistent luminescence and decay characteristics have been studied. The material doped with Mn<sup>2+</sup> ions gives intense wide emission band from 610 nm to 780 nm with maximum emission intensity at 690 nm (λ<sub>exc</sub>= 412 nm), which is ascribed to the forbidden d-d transition of Mn<sup>2+</sup> from the <sup>4</sup>T<sub>1</sub> to <sup>6</sup>A<sub>1</sub> energy states. Co-doping of Tm<sup>3+</sup> further causes a splitting of broad band at around 670 nm and at 694 nm.

The material shows excellent persistent luminescence in blue (if  $\text{Tm}^{3+}$  is doped only, ZPOT), red (if  $\text{Mn}^{2+}$  is doped only, ZPOM) and NIR region (both  $\text{Mn}^{2+}$  and  $\text{Tm}^{3+}$  are co-doped, ZPOT:2xM). Long lasting phosphorescence (LLP) emission spectra of the samples ZPOT:2xM ( $0 \leq x \leq 0.05$ ) is shown in Fig. 7(A). Characteristic blue LLP emissions of  $\text{Tm}^{3+}$  peaking at 368 nm ( $^1\text{D}_2 \rightarrow ^3\text{H}_6$ ), 454 nm ( $^1\text{D}_2 \rightarrow ^3\text{H}_4$ ) and 482 nm ( $^1\text{G}_4 \rightarrow ^3\text{H}_6$ ), respectively is observed in  $\text{Tm}^{3+}$  singly doped material. However, in the ZPOT:2xM samples, the intensity of the blue LLP emissions of  $\text{Tm}^{3+}$  decreases gradually with increasing concentration of  $\text{Mn}^{2+}$  and finally disappears when the value of  $x$  exceed 0.005. This results in the intensity enhancement of the red emission of  $\text{Mn}^{2+}$  which attains maximum value at  $x = 0.01$ . In addition, a longer wavelength shift of emission maximum of  $\text{Mn}^{2+}$ , from about 625 nm to 690 nm, is also observed, which is explained due to the two possible distinct Zn sites in the structure of  $\alpha\text{-Zn}_2\text{P}_2\text{O}_7$ . Thus, the change of the emission intensity ratio of 625 nm to 690 nm band leads to a colour shift of  $\text{Mn}^{2+}$  LLP from red to NIR. Fig. 7(B) describes the LLP decay curves monitored for the emissions of  $\text{Mn}^{2+}$  at 690 nm. LLP decay curve of  $\text{Mn}^{2+}$  exhibits a third exponential decay process, obeying the decay function

$$I = A_1 \exp(-t/\tau_1) + A_2 \exp(-t/\tau_2) + A_3 \exp(-t/\tau_3),$$

Where,  $I$  is phosphorescence intensity;  $A_1$ ,  $A_2$  and  $A_3$  are constants;  $t$  is time;  $\tau_1$ ,  $\tau_2$  and  $\tau_3$  are decay times for exponential components, respectively. Obtained value for  $\tau_1$ ,  $\tau_2$  and  $\tau_3$  are 4.1 s, 25.1 s, and 135.2 s, respectively. Fig. 7(B) also contains the LLP decays as a function of inverse of LLP intensity ( $I^{-1}$ ) versus time ( $t$ ), through which authors explain the tunnelling process of electrons transferring from defects to the activator ions.

Similarly, Li *et. al.* studied the NIR luminescence of  $\text{Mn}^{4+}$  in La and Gd based aluminates and propose a holistic design concept for NIR long persistent phosphors.<sup>129</sup> Samples were synthesized using typical solid state reaction method and characterized for phase, microstructure, photoluminescence, persistent luminescence, decay curves, defect

properties using TL and ESR studies, *etc.* Mn<sup>4+</sup>-doped MAIO<sub>3</sub> (M=La, Gd) persistent phosphors gives emission maximum around 730 nm. Different concentrations of Mn<sup>4+</sup> and Ge<sup>4+</sup> have been used and their effect on persistent emission has been studied. Co-doping of Ge<sup>4+</sup> tailors the defect level trap depths and thereby a considerable improvement of persistent time over 20 h has been attained for the sample La<sub>1</sub>Al<sub>0.99</sub>O<sub>2.985</sub>:0.1%Mn<sup>4+</sup>, 0.9%Ge<sup>4+</sup> (LAM21) and Gd<sub>1</sub>Al<sub>0.99</sub>O<sub>2.985</sub>:0.1%Mn<sup>4+</sup>, 0.9%Ge<sup>4+</sup> (GAM 23). NIR long persistent luminescence of both the samples GAM23 and LAM21 (Fig. 7(C)) phosphors were detectable by supersensitive camera even up to 24 h, after pre-irradiation of the samples by 325 nm radiation of Xe flash lamp for 10 min. The materials were used for imaging applications also. Fig. 7(D) shows the deep tissue images of pork tissues injected with GAM23 phosphor. For imaging, phosphors were first irradiated with 325 nm light of Xe flash lamp for 10 min and then injected in tissues. Authors claim that, phosphors gives a very high resolution even after 2 h post-injection, due to the absence of auto-fluorescence and higher signal-to-noise ratio. This allows tissue bioimaging to be monitored for more than 12 h. Few other works on Mn doped NIR persistent phosphor material may also be found, but, as far as the bioimaging application is concerned the above mentioned works are the representative works in the area and are signpost for researchers working in this area to plan and design further developments. In the next step towards the development of efficient NIR persistent phosphor for bioimaging applications, in last few years, Cr<sup>3+</sup> doped persistent materials have been widely explored. The works are summarized in next section.

### 4.3 Cr<sup>3+</sup> doped persistent materials and bioimaging

The electronic configuration for Cr<sup>3+</sup> is 1s<sup>2</sup>2s<sup>2</sup>2p<sup>6</sup>3s<sup>2</sup>3p<sup>6</sup>3d<sup>3</sup>, recall that ionization of an atom expels an electron from the orbital with highest principle quantum, thus, the Cr<sup>3+</sup> ion is a d<sup>3</sup> ion. These three electrons are distributed among the five 3d orbitals, depending upon the environment in which the ion exists. The ground state terms are <sup>4</sup>F, <sup>4</sup>P, <sup>2</sup>G, <sup>2</sup>H, <sup>2</sup>P, <sup>2</sup>D, *etc.*

Similar to the case of  $\text{Mn}^{2+}$ , many of these levels split into two or more levels; the degeneracy of them is represented by  $2L+1$ . These crystal field modified degenerate energy levels are represented by  $^{2S+1}X$ , where X usually correspond to A for no degeneracy, E for a two-fold degeneracy and T for a three-fold degeneracy. The NIR emission in  $\text{Cr}^{3+}$  is observed due to the spin forbidden  $^2E \rightarrow ^4A_2$  transition, or a broadband emission (650-1600 nm) due to the spin-allowed  $^4T_2 \rightarrow ^4A_2$  transition, which strongly depends on the crystal-field environment of the host lattices. Herein,  $^4T_2$  excited state strongly depends on crystal/ligand field, e.g. in a tetrahedral symmetry, the  $^4T_2$  excited state lies below the  $^2T_1$  and  $^2E$  excited states and gives rise to a broad-band NIR emission via radiative transition to ground state  $^4A_2(F)$ . Therefore, the NIR emission wavelength from  $\text{Cr}^{3+}$  can be controlled by modifying the ligand field strength. Further defect levels/traps plays important role to make the emission long persistence. Keeping this in view,  $\text{Cr}^{3+}$  has been studied for NIR persistent luminescence in different crystal lattices, mainly in  $\text{ZnGa}_2\text{O}_4$  and substituted structures, to vary the crystal field strength. Table 3 lists the detail of different hosts, emission wavelength, and duration of persistent luminescence (in h) of NIR persistent materials activated with  $\text{Cr}^{3+}$ .<sup>41,50,130-154</sup> On the basis of the available research articles the detailed overview may be given in following sub-sections.

#### 4.3.1 Zinc-Gallate ( $\text{ZnGa}_2\text{O}_4$ ) nanostructures and bioimaging

$\text{Ga}_2\text{O}_3$  based wide band gap materials are considered to be one of the most applicative wide band gap materials, not only in its intrinsic phase but also in many other phases particularly with alkali, alkaline or with some transition metals, lanthanides, *etc.* For persistent luminescence purpose, Zn based Gallates, e.g.  $\text{ZnGa}_2\text{O}_4$ , is of great interest now a days as it exhibits different emission colours when doped with transition metal elements and is chemically and thermally stable wide band gap semiconductor.<sup>130-136</sup> After the first report on NIR persistent luminescence in  $\text{Cr}^{3+}$ -doped  $\text{ZnGa}_2\text{O}_4$  by Bessiere *et. al.* in 2011, this material

have been attracting the most attention, particularly for bioimaging applications.<sup>130</sup> The detailed study on this host is further subdivided as follows.

#### 4.3.1.1 Structure of zinc Gallet

As far as the structure is concerned,  $\text{Ga}_2\text{O}_3$  is of polymorphism in its crystal structure. The polymorph of  $\text{Ga}_2\text{O}_3$  mainly includes  $\alpha\text{-Ga}_2\text{O}_3$  (R3m,  $a=4.979 \text{ \AA}$  and  $c=13.429 \text{ \AA}$ ),  $\beta\text{-Ga}_2\text{O}_3$  (C2/m,  $a=12.23$ ,  $b=3.04$ ,  $c=5.80 \text{ \AA}$ , and  $\gamma\text{-Ga}_2\text{O}_3$  (Fd3m,  $a=8.22 \text{ \AA}$ ). Of those phases, the  $\beta\text{-Ga}_2\text{O}_3$  is only stable modification.<sup>155-158</sup> Whereas zinc Gallet,  $\text{ZnGa}_2\text{O}_4$  (ZGO), is an  $\text{AB}_2\text{O}_4$  compound with spinel structure, in which  $\text{Zn}^{2+}$  and  $\text{Ga}^{3+}$  ions occupy tetrahedral A and octahedral B sites, respectively, Fig. 8(a). Despite the fact that it is most generally considered as a typical spinel, it shows a slight reversal character as well, so that a few percent of  $\text{Zn}^{2+}$  and  $\text{Ga}^{3+}$  occupy B and A sites, respectively. Such defects in the host matrix are called antisite defects and so a Zn ion goes at a Ga site and a Ga ion goes at a Zn site (noted as  $\text{ZnGa}'$  and  $\text{GaZn}^\circ$  in Kröger-Vink notation, respectively) in an ideal normal spinel structure type. ZGO displays about 3% inversion, which implies that 3% of  $\text{Zn}^{2+}$  involve Ga destinations, and correlatively the same measure of  $\text{Ga}^{3+}$  possess Zn sites.<sup>132,159,160</sup>

#### 4.3.1.2 Photoluminescence excitation, emission and persistent luminescence

Photoluminescence excitation spectrum of  $\text{Cr}^{3+}$  doped samples (for its well known emission at around 700 nm) shows four important regions which all together covers UV and visible spectral regime. The first broad excitation band is observed below 250 nm, due to  $\text{O}^{2-}\text{-Ga}^{3+}$  charge transfer band. The second excitation band arises due to band-to-band transition at around 290 nm. Rest of the two bands, in the visible region (425-570 nm), appears due to d-d transitions of  $\text{Cr}^{3+}$  ion.<sup>130-136</sup> Bessiere *et. al.* have studied emission by exciting into all these three distinct excitation bands, Fig. 8(b).<sup>132</sup> They observed that, the  ${}^2\text{E}(2\text{G}) \rightarrow {}^4\text{A}_2(4\text{F})$  transition of  $\text{Cr}^{3+}$  in an octahedral crystal field is composed of a large number of peaks. It has been explained due to two different sites for  $\text{Cr}^{3+}$  ions in this crystal structure, i)  $\text{Cr}^{3+}$  in

unperturbed octahedral sites (denoted as CrR) and ii)  $\text{Cr}^{3+}$  ions with a neighbouring antisite defect (denoted as CrN2). The peak corresponding to zero phonon R lines (for CrR) is observed at around 688 nm, while, peak corresponding to zero phonon N2 lines (for CrN2) is observed at around 695 nm. Stokes and antiStokes phonon side bands (PSB) associated with zero phonon lines have also been reported. Sharp peaks at 708 and 715 nm (Stokes) and 663, 670, and 680 nm (antiStokes) have been reported for R lines. PSB for N2 lines are observed in 650-750 nm regime, however, it appears with relatively weak intensity. These zero phonon line and associated PSB give rise to a broad band from 650 nm to 750 nm composed of large number of sharp peaks.  $\text{Cr}^{3+}$  ions with a neighbouring antisite defect (CrN2) play an important role for persistent luminescence. Fig. 8(b) shows the persistent luminescence spectrum of the  $\text{Cr}^{3+}$  doped zinc Gallet after few seconds of stoppage of excitation at 290 nm for 15 minutes. The spectrum is dominated by N2 line. The decay curves after 290 nm and 550 nm excitation are also shown in Fig. 8(c).

#### 4.3.1.3 Mechanism involved in persistent luminescence

If one looks towards the mechanism involved for the persistent luminescence of  $\text{Cr}^{3+}$  in zinc Gallets, several models have been proposed by different groups and it seems difficult enough to get a conclusive remark. Recently, Zhaung *et. al.* discussed this issue in his paper very clearly.<sup>133</sup> They marked that, there are two major controversial points in proposed models so far- (i) species of charge carriers (whether a negative electron or a positive hole), and (ii) path of the trapping process (whether through the conduction band or through the valence band or by a quantum tunnelling effect in the band-gap). They simplify it by an energy level diagram, shown in Fig. 8(d). According to this energy level, there are three ways by which electron can be excited to the conduction band (CB): (i) from ground state (GS) to excited state (ES) situated above the bottom of the CB; (ii) directly from GS to CB; (iii) from GS to ES situated below the bottom of the CB. In the third case, the electron can reach to the CB with thermal

energy, which is called thermally assisted photoionization process. The population from the CB is further moved to the trap centre. This trapping mechanism has been mostly adopted by many authors. But, quantum tunnelling (QT), another possible path for electron trapping, cannot be completely ignored. These trap charges give rise to the persistent luminescence after the removal of excitation source either through thermal excitation (possible even at room temperature) and/or by photo-stimulation with suitable frequency of light.

The paper additionally remarks on to how one can effectively find out the relative locations of VB and CB of the host, GS and ES of the luminescent centre, and position of trap levels by making use of different characterization techniques, which is most extreme prerequisite to propose a right mechanism involved in the persistent luminescence process. The energy of the topmost level of the VB may be characterized as zero by embracing the idea of a host referred binding energy (HRBE) scheme. Further the absorption spectra of an un-doped sample (host) could be used to determine the band-gap energy, which would give the information about the position of CB bottom. Further, photoconductivity excitation (PCE) spectra, persistent luminescence excitation spectra (PersLE), or photoluminescence excitation (PLE) spectra measurements can be used to evaluate the energy of the electronic transition from the GS to the bottom of the CB. Similarly, for the transition metal doped samples, absorption spectra or PLE spectra can confirm 3d-3d intra-transitions from GS to various ES. At last, the depth of defect/trap levels (for stimulation: thermal activation energy, or photostimulation) can be attained through thermoluminescence (TL) glow curve measurement.<sup>133</sup>

#### **4.3.1.4 Nanoparticles, surface functionalization and bioimaging**

Even after the first report of persistent luminescence in  $\text{Cr}^{3+}$  doped  $\text{ZnGa}_2\text{O}_4$ , in 2011, bioimaging application of this material first came in 2014 only. This was due to the fact that, substituted structure of zinc Gallate e.g. zinc gallogermanate was found to be more efficient in

terms of persistent luminescence intensity and persistent time both and so it drawn more attention and used successfully for imaging application much earlier, discussed in detail in the next section 4.3.2. However, the group, which first reported the NIR persistent luminescence by  $\text{Mn}^{2+}$  doped phosphor for imaging application, made the first use of zinc Gallet phosphor for imaging application also, and found it suitable for optical imaging of vascularization, tumours and grafted cells for the first time.<sup>134</sup>

NPs of the zinc Gallet phosphor (ZGO) were prepared using hydrothermal method followed by low-temperature sintering in air. Hydroxylation of these NPs was performed by basic wet grinding of the powder (ZGO-OH). Further surface functionalization were done according to their earlier protocol in case of  $\text{Mn}^{2+}$  doped silicate with a small modification to get ZGO-NH<sub>2</sub> and ZGO-PEG, scheme shown in Fig. 9(a). Fig. 9(b) shows the TEM image of NPs with a core diameter of 20-60 nm. As compared to the ZGO-NH<sub>2</sub>, PEG grafting increases hydrodynamic diameter (80 nm) and causes an opposite shift in zeta potential (-6.70 mV) (see Fig. 9(c, d)), but, optical characteristics remains same for both types of particles. Remarkably, surface functionalization with PEG helps colloidal solution of NPs to remain in blood circulation for longer time.

PEG functionalized particle were able to circulate in blood circulation root for more than 2 h, which favours tumour targeting *in vivo* and the group successfully demonstrated first proof of *in vivo* tumour passive targeting. Initially during the first 2 h bio-distribution of ZGO-PEG was similar for tumour-bearing and healthy mice both and tumours were not visible; however, after 4 h tumours were clearly visible, indeed NPs need activation by orange/red source (photo-stimulation) after such a long period. Luminescence from regions of interest (ROIs) was compared with the global luminescence signal from the entire animal which shows only a little variation in intensity from tumours (subcutaneous CT26) due to permeability and retention effect; however, a significant enhancement in intensity by liver

(from 18% to about 50%) is observed during 6 h which confirms for a major accumulation of stealth NPs within liver (Kuffer cells). The result is summarized in Fig. 10(a-e). Heavy accumulation of the particles in liver after 6 h strained authors to further examine the cellular and systemic toxicity of these ZGO-based PLNPs to answer the biocompatibility issue of the used NPs. Importantly, there was no any signature of inflammation or any change in morphology during histopathology even after 24 h of injection of NPs, which, although preliminary, confirms that ZGO-PEG NPs are free from acute toxicity in healthy mice.

Finally, authors investigated the use of surface functionalized ZGO NPs (ZGO-OH, ZGO-NH<sub>2</sub> and ZGO-PEG) to track injected cell (RAW264.7 macrophages) *in vivo*. In this context first they performed preliminary investigation regarding suitable NPs, internalization of NPs in the cell, and of course the cell viability too. ZGO-NH<sub>2</sub> NPs underwent superior phagocytosis with a clearly detectable persistent luminescence, after orange/red excitation (photo-stimulation). In addition to this, incubation with ZGO-NH<sub>2</sub> does not show significant affect on cell viability too, results are summarized in Fig. 11(a-c). Efficient internalization was clearly verified through confocal microscopy (Fig. 11(d-f)) and TEM measurements. After confirming these, bio-distribution of free ZGO-NH<sub>2</sub> was compared with the bio-distribution of RAW 264.7 cells incubated with ZGO-NH<sub>2</sub> NPs. As pointed our earlier, free NPs are accumulated mostly in liver and spleen (RES organ), however, on the other hand, labelled cells led to a strong luminescence signal in the lungs due to rapid sequestration of phagocytes in the lung capillary bed (shown in Fig. 11(g, h)). This different behaviour was further verified by *ex vivo* persistent luminescence acquisition 24 h after intravenous injection also (shown in Fig. 11(i)).

#### 4.3.2 Ge/Sn substituted zinc-Gallate (ZnGa<sub>2</sub>O<sub>4</sub>) nanostructures and bioimaging

Cr<sup>3+</sup> doped ZnGa<sub>2</sub>O<sub>4</sub> was found to be an excellent NIR emitting material, particularly probed for bioimaging application. The persistent time was found to be few hours only, however,

through photostimulation by LEDs for a small period may recover persistent emission and can complement the process for long period imaging applications also. But, at the same, it strained researchers to improve afterglow time so as to exploit their wide applications; and so Ge/Sn/Al substituted zinc Gallates were developed further.<sup>41,50,137-140</sup> Pan *et. al.* (in 2012) came with an innovative composition which holds persistence time > 360 h.<sup>137</sup> Herein, persistence time refers to the duration for which an eye can see with the aid of a night-vision monocular in a dark room. In their new composition, they substituted Ga by Ge and suggested a general chemical formula  $Zn_xGa_yGe_zO(x+(3y/2)+2z):tCr^{3+}, mR$ , where R is a co-dopant selected from a group consisting of alkaline earth ions, lanthanide ions and  $Li^+$  ions; x, y and z are integers from 1 to 5; t is 0.01 to 5 mol%; and m is 0 to 5 mol% of the  $Cr^{3+}$ -doped zinc gallogermanates. Detailed excitation, emission, decay curve and thermoluminescence measurements have been carried out to explore different properties. Fig. 12 shows persistent decay curves and persistent luminescence spectra (a) along with beautiful digital photographs of the persistent emission at different time interval (b-h) for  $Zn_3Ga_2Ge_2O_{10}:0:5\%Cr^{3+}$  phosphor. Persistent emission is although weak even clearly visible upto 360 h, which recover the initial intensity again after heating, i.e. by thermal stimulation, (Fig. 12(i)). The other beauty of this material was its activation by Sunlight in different outdoor conditions such as different weather conditions (Sunny, cloudy, overcast and rainy days), at different moments between Sunrise and Sunset and at various outdoor locations (for example, in open areas and shadows of trees and buildings), *etc.* Moreover to this, persistent luminescence retained even in aqueous solutions including tap water, salt (NaCl) water and NaCl/bleach/bicarbonate ( $NaHCO_3$ ). Authors suggested different potential applications of this material such as in night surveillance, photovoltaics including *in vivo* imaging. Bioimaging application of this material was further realized by different researchers in subsequent years.<sup>41,50,139</sup>

Li *et. al.* used Cr<sup>3+</sup> doped zinc gallogermanates for imaging of pork tissue with incoherent excitation.<sup>41</sup> The group initially verified well established facts such as the existence of defect states through ESR measurement. The ESR peak appears at a g-value of 1.9996 (3374.9 G) which persist for an extended period >6 h. Also, further through PCE measurement at different temperature (in the range 20-300K) they confirm the possibility of energy charging of this material by UV-visible light (250-450 nm). A detailed excitation, emission and decay characteristics have been presented. Additionally group demonstrates stability and reproducibility of the antiStoke luminescence of the material through continuous irradiation with a LED and through cyclic operation over 17 individual on/off cycles of 10 min. Finally, for imaging application NPs were dispersed in ordinary saline (100 mg/ml) and injected into tissue at various injection depths (0.1-1 cm). Charging was performed *ex situ* (Xenon short-arc lamp) as well as *in situ* (X-ray activated) and photostimulation was done by IR LED (980 nm and 940 nm). The probe signal was clearly detectable in both the cases. Activation was possible for large-area (6 cm<sup>2</sup>) as well as for deep penetration depth (1 cm). A good cellular viability (>95 %), in the presence of injected NPs with a concentration of 100 mg/cm<sup>2</sup>, and thus a low toxicity of the employed probe was clearly visible through cytotoxicity studies. In a similar work, likewise the substitution by Ge, Sn was used (Zn<sub>3</sub>Ga<sub>2</sub>Sn<sub>1</sub>O<sub>8</sub>:0.5 Cr<sup>3+</sup>) which gives almost equally good persistence time of over 300 h.<sup>50</sup> Along with all the essential studies, such as optical properties, trap level analysis, photostability, persistent luminescence characteristics, bioimaging and cytotoxicity studies have also been carried out. Bioimaging have been carried out on goldfish. NIR persistent luminescence could be clearly imaged for about 2 h, which on photostimulation, through NIR LEDs, recover the initial intensity of persistent emission.

The work of Abdukader *et. al.* also reports bioimaging with zinc gallogermanates doped with Cr<sup>3+</sup>.<sup>138</sup> The novelty includes following major changes, i) co-doping of a

lanthanide  $\text{Pr}^{3+}$  ion and creating suitable Zn deficiency in zinc gallogermanate (ZGGO) host, ii) bioconjugation of PEG modified NPs with c(RGDyK) peptide further, and iii) extensive toxicity study covering *in vitro* (on 3T3 normal cell lines and U87MG cancer cell lines by cell counting assay) and *in vivo* (monitoring histological changes in several susceptible organs including heart, liver, spleen, lung, and kidney) as well as acute (7 days) and chronic (30 days) toxicity. The first change let them get a suitable host composition ( $\text{Zn}_3\text{Ga}_{1.96}\text{Ge}_2\text{O}_{10}:\text{Cr}_{0.01}\text{Pr}_{0.03}$ ) which could give intense persistent luminescence for more than 15 days. Herein,  $\text{Pr}^{3+}$  adjusts the trap density and trap, while control over zinc content facilitates persistent energy transfer between host emission and  $\text{Cr}^{3+}$  ions, which altogether results to prolong afterglow. Secondly, PEGylated NPs were obtained, as already reported in other works, to increase the blood circulation time. Further, one step ahead, PEGylated NPs were conjugated with a RGD peptide-c(RGDyK) to perform tumour-targeted imaging application. Complete surface functionalization steps are shown in Fig. 13(A).

PEG functionalized NPs, administered into a normal mouse through subcutaneous injection, show excellent persistent luminescence and allow *in vivo* bioimaging to be monitored (with  $\text{SNR} > 5$ ) for more than 15 h. NIR stimulation by 980 nm laser light recovers persistent luminescence after 5 days which further retains even after 11 days, which shows the suitability of material for long-term *in vivo* imaging via repeated stimulation with NIR light. Likewise the earlier report for biodistribution, the material is mainly accumulated in RES organs, persistent luminescence through which was still visible for about 450 min (7.5 h) after injection. Further tumour targeting was carried out both by PEG-LPLNPs and RGD-LPLNPs (for a comparative study) by injecting the material into U87MG tumour-bearing mice and normal mice. Both the materials were able to mark the tumour site (see Fig. 13(B, a-d)), but the luminescence signal from RGD-LPLNPs was visible for longer time in tumour site. This was due to the high affinity of the RGD-LPLNPs to inter in  $\alpha_v\beta_3$  on tumour

vasculature. *Ex vivo* imaging of the different organ including tumour was also performed and the persistent luminescence from tumour was clearly visible, Fig. 13(B-e).

Thus, in summary, Ge/Sn/Al substitution in  $\text{ZnGa}_2\text{O}_4$  significantly improves the persistent emission intensity and persistent time as a result of which the imaging is better performed in terms of long time imaging and targeting both.

#### 4.3.3 Lithium Gallet ( $\text{LiGa}_5\text{O}_8$ ) nanostructure and bioimaging

Another material of interest, i.e.  $\text{Cr}^{3+}$ -doped  $\text{LiGa}_5\text{O}_8$ , in this continuation, bearing the excellent NIR persistent luminescence (persistent time more than 1000 h) under visible light or a NIR light stimulation, was reported by Liu *et. al.*<sup>141</sup> They pointed out different promising applications viz. optical information storage, night-vision surveillance including *in vivo* bioimaging of this material. To demonstrate the potential of material for *in vivo* bioimaging, NPs (particle diameter of the order of 50-150 nm) were prepared by using sol-gel method followed by high-temperature calcination, and further surface functionalization of these NPs was done by using polyethylenimine (PEI). In the next step, these functionalized NPs were used to label 4T1 murine breast cancer cells. This system was charged with 254 nm UV lamp and then injected subcutaneously into the back of a nude mouse. Persistent luminescence was monitored at different time interval with and without photostimulation. Persistent luminescence was clearly visible upto 4 h after the injection, Fig. 14(a), and then after fade up. However, stimulation by a white LED flashlight recovers/rejuvenates NIR persistent luminescence. Fig. 14(a1-e1) and (a2-e2) shows the images of persistent luminescence, after stimulating the sample by white LED for 15 s, 10 s, and 5 min after the stimulation. It is obvious that the resulting persistent luminescence signals retain sufficient intensity for more than 5 min (Fig. 14a2-e2). Thus by repeated stimulation authors were able to continue imaging possible even up to 10 days after the injection. Some other authors have also worked on similar host composition and found them suitable for bioimaging

applications.<sup>142,143</sup> Abdukayum *et. al.* compared this material with zinc gallogermanate codoped with Cr and Pr and found that, the latter one is more suitable in many ways for imaging applications.<sup>138</sup>

#### 4.3.4 Miscellaneous host

In spite of lithium Gallet, zinc Gallet and its substituted structures, several other host matrices doped with Cr<sup>3+</sup> ions were also developed meanwhile for realising NIR persistent luminescence from them. Few important materials such as gallium oxide,<sup>144-145</sup> alkaline Gallets,<sup>146-148</sup> lanthanide garnets,<sup>149-151</sup> and lanthanum gallogermanates,<sup>152,153</sup> aluminates<sup>154</sup> also gives NIR persistent emission but as far as the imaging application from them is concerned, it is still not explored. Lu *et. al.* reported NIR persistent emission from hydrothermally synthesized  $\beta$ -Ga<sub>2</sub>O<sub>3</sub>:Cr<sup>3+</sup> nanowire assemblies and speculate its potential applications as identification taggants in security and optical probes in bioimaging.<sup>144</sup> While, Wang *et. al.* shows the photocatalytic properties from Ga<sub>2</sub>O<sub>3</sub>:Cr<sup>3+</sup><sub>0.01</sub>, Zn<sup>2+</sup><sub>0.005</sub> persistent phosphor.<sup>145</sup> Magnesium and strontium Gallets have been claimed as new phosphor for *in vivo* imaging, but not implemented so far.<sup>146-148</sup> Similar is the case with other works also which focus on to structural and optical characteristics and on the basis of results speculate their possible application in *in vivo* imaging, *etc.* It would be exciting to see a novel composition in this line with better performances than existing materials usable for bioimaging applications.

#### 5.0 NIR persistent phosphor and multimodal imaging

Every specific imaging technique has its own particular peculiarity of benefits and certain constraints too, so more than one imaging strategy (also called multimodal imaging) are utilized sooner or later for more precise, complete, and dependable data on diagnosis. In this context, Abdukayam *et. al.* put forward the idea to develop NIR PLNPs for multimodal imaging, both exhibiting NIR fluorescence imaging and magnetic resonance imaging as well.<sup>51</sup> The NIR fluorescence imaging is excellent for high sensitivity, while its limitation

towards poor spatial resolution can be complemented with MRI.<sup>161,162</sup> To realise this concept, zinc gallogermanates ( $\text{Zn}_{2.94}\text{Ga}_{1.96}\text{Ge}_2\text{O}_{10}$ ) doped with  $\text{Cr}^{3+}$  and  $\text{Pr}^{3+}$  was developed as NIR PLNPs and further it was chelated with Gd ions to obtain Gd(III)-PLNPs. The material was found safe under *in vivo* and *in vitro* toxicity tests as well.

The process of chelation involves surface coating of NPs with APTES (3-amino propyltriethoxysilane, amino functional group), binding of diethylenetriamine pentaacetic acid (DTPA), through 1-ethyl-3-(3-(dimethylamino)propyl)-carbodiimide hydrochloride (EDC-HCl), and N-hydroxysuccinimide (NHS) coupling reaction, to these amino groups followed by chelation with Gd(III). Persistent luminescent emission and decay characteristics of the aqueous solution of the as-synthesized Gd(III)-PLNPs was investigated compared with PLNPs. Although persistent luminescence intensity and persistent time both are effected by surface modification with the gadolinium complexes, yet, it was excellent enough for imaging application, NIR persistent luminescence (for the solution with Gd(III)-PLNPs concentration,  $1 \text{ mg mL}^{-1}$ ) was detectable even after 24 h after stopping excitation with  $\text{SNR} = 5.2$ . Further to evaluate the capability of this material for MRI, longitudinal proton relaxation times (T1) was determined and compared with commercial Gd-DTPA complex, which was found better for the case of synthesized Gd(III)-PLNPs material. This confirmed the potential of Gd(III)-PLNPs as an effective contrast agent for T1-weighted MRI also.

Authors successfully demonstrated the use of this material for *in vivo* NIR luminescence imaging (Fig. 15(a)) as well as for *in vivo* T1-weighted MRI (Fig. 15(b)). For the first type, Gd(III)-PLNPs solution ( $1 \text{ mg mL}^{-1}$ ) was excited using 254 nm UV lamp for 10 min and then injected (intravenous, 300  $\mu\text{L}$ , PBS) into mouse. Imaging was possible for more than 6 h ( $\text{SNR}=5$ ) with a major luminescence signal from liver sites (Fig. 15(a)). This clearly demonstrates that, the Gd(III)-PLNPs are capable of long-term *in vivo* imaging without *in situ* excitation. Further, *in vivo* T1-weighted MRI of Kunming mice was

performed before and after intravenous injection of Gd(III)-PLNPs solution (300  $\mu\text{L}$ , 1 mg  $\text{mL}^{-1}$ ) on a 1.2 T MRI system. Spatial resolution was better with MRI. The liver of the mouse was not very clear for preinjection mouse, however, visibility is significantly pronounced after 15 min postinjection of Gd(III)-PLNPs (Fig. 15(b)). Thus, successful demonstration of both the imaging techniques probes the multimodality of the material.

In another work by Chen *et. al.* calcium gallogermanate ( $\text{Ca}_3\text{Ga}_2\text{Ge}_3\text{O}_{12}$ ) have been synthesized codoped with  $\text{Cr}^{3+}$  ion and  $\text{Tm}^{3+}$ ,  $\text{Yb}^{3+}$  ions.<sup>163</sup> Authors successfully observed NIR persistent luminescence due to  $\text{Cr}^{3+}$  ion (with persistent time of about 2 h) and NIR to NIR upconversion emission due to  $\text{Tm}^{3+}$ ,  $\text{Yb}^{3+}$  ion couple. Interestingly, co-doping of  $\text{Tm}^{3+}$  enhances the persistent luminescence also. Authors suggest its potential application in imaging both through persistent luminescence as well as through UC, but admit that still a long distance remains to traverse to achieve this goal. Thus, in summary, already some research work have been started to introduce multimodality in persistent phosphor, but the results are preliminary and needs further attention to develop efficient material which could meet the pragmatic aspects of multimodal imaging applications.

## 6.0 Summary and outlook

The introductory aspect of the review starts with prologue on bioimaging in general and optical imaging in particular and finally focuses onto most recently explored NIR emitting persistent luminescence nanoparticles (PLNPs) for bioimaging application. Accordingly, a prerequisite towards better understanding of the subject makes it vital to talk about persistent luminescence, its development, present status of the field, literary review of the existing red and NIR emitting persistent phosphors, *etc.* The significant finding on NIR persistent luminescence and its application for bioimaging are based on transition metals, primarily either on  $\text{Mn}^{2+}$  and/or on  $\text{Cr}^{3+}$  as one of the dopant/co-dopant ion. Other than these two

fundamental classes of activators, barely any other ions have been found to exhibit persistent luminescence in NIR region usable for bioimaging application.

$\text{Mn}^{2+}$  doped silicates ( $\text{Ca}_{0.2}\text{Zn}_{0.9}\text{Mg}_{0.9}\text{Si}_2\text{O}_3: \text{Eu}^{2+}, \text{Dy}^{3+}$ ) were first identified suitable NIR persistent phosphor for imaging application. Trap centres in this material is created due to  $\text{Dy}^{3+}$  doping and lanthanide ions act as primary acceptor of energy, which is thermally released to  $\text{Mn}^{2+}$  ions, through tunnelling and persistent energy transfer processes. The change in composition brings out changes in the symmetry and crystal field strength around  $\text{Mn}^{2+}$  site which is responsible for emission from red to NIR corresponding to well known  ${}^4\text{T}_1(4\text{G})$  excited state to the  ${}^6\text{A}_1(6\text{S})$  fundamental state. Biodistribution of these NPs, which depends significantly on surface charge, is improved by surface functionalization with poly ethylene glycol (PEG). Blood retention capability highly depends on core diameter of the NPs as well as on surface coating, thus methoxy-PEG modified NPs were identified more suitable to improve tumour targeting in mice. In addition to this, functionalization of PEG-PLNPs with small molecules such as biotin and Rak-2 make it useful to even target malignant glioma cells and prostate cancer cell, respectively. Thus the material was good enough for different imaging and targeting applications, however, improvement in the emission intensity/persistent time was realised essential for long-term and deep tissue monitoring of *in vivo* probe accumulation, which leads to the development of  $\text{Cr}^{3+}$  doped nanostructures. In the next step,  $\text{Cr}^{3+}$  doped zinc based Gallates and substituted structures attracted the major attention due its excellent NIR persistent emission with a longer afterglow time for more than 2 weeks. More than this, the persistent emission can be rejuvenated/recovered by photostimulation, especially by incoherent light sources (e.g. LEDs) which offers real time long term imaging application of these PLNPs. Although, the concept evolved recently (first reported in 2011), the theory developed successfully address wide aspects related to structure

of the material, effect of structure on the persistent luminescence of  $\text{Cr}^{3+}$  ions, photostimulation, surface functionalization, imaging, toxicity, *etc.*

Important findings can be summarized as follows. The basic requirement in such materials is to generate suitable trap levels. Existence and localization of such defects states could be estimated through electron spin resonance (ESR) and thermoluminescent (TL) glow measurements. The peak temperature and full width at half maximum (FWHM) of the TL glow curves reflect the trap depth and the trap depth distribution. In the next step, charging, emission and processes involve in between become important. Photocurrent excitation (PCE) measurement can be used to find out information about the energy charging range for a particular material, which basically lies in UV-visible regime for gallogermanates. Routine excitation, emission and decay curve analysis can be applied for photoluminescence and persistent emission measurement. Persistence time is a technical term here, which refers to the duration for which an eye can see with the aid of a night-vision monocular in a dark room. Bioimaging involves surface functionalization, bio-distribution and targeting applications which is somewhat similar to that of  $\text{Mn}^{2+}$  doped material, indeed with better resolution, high signal to noise ratio, longer retention time in blood circulation and better targeting ability, *etc.* Both acute and chronic toxicity in *in vivo* and *in vitro* studies shows that these particles are safe for bioimaging application.

In conclusion,  $\text{Cr}^{3+}$  doped zinc gallogermanates NIR PLNPs has evolved as most adaptable and easy to use optical nanoprobe. These PLNPs emits intense, long-lasting persistent light even after the removal of the excitation which allows imaging without external excitation and completely removes the possibility of auto-fluorescence/background noise and thus improves signal-to-noise ratio and sensitivity greatly. Further, emission in NIR region by  $\text{Cr}^{3+}$  lies in the tissue transparency window which further increases the detection depth. Notwithstanding this, plausibility of photo-stimulation by incoherent light source,

LEDs)/flash lamps, makes long term imaging conceivable, which is off base simpler, financially savvy and safe. Taking into account the recent improvements in NIR persistent phosphors, a guaranteeing future for this material might be predicted especially for scientists and pharmacologists involved in numerous distinctive sorts of researches related to cancer diagnosis, vascular biology and cell researches, *etc.*

The majority of the reported NIR PLNPs covers NIR I region, therefore, it would be of future viewpoint to develop persistent phosphor for NIR II region also and look for their response in imaging and targeting applications. Notwithstanding this, further investigation and endeavours to develop multimodal persistent phosphors, for example which may work both as optical as well as magnetic probe will certainly be exciting for future course of researches.

### Acknowledgements

Author thankfully acknowledges financial support from Department of Science and Technology (DST), New Delhi, India through its DST-INSPIRE Faculty award (IFA-12 PH-21) program.

### References

- 1 R. C. Weissleder and M. J. Pittet, *Nature*, 2008, **452**, 580-589.
- 2 J. Xie, G. Liu, H. S. Eden, H. B. Ai and X. Y. Chen, *Acc. Chem. Res.* 2011, **44**, 883-892.
- 3 D. L. Daugherty and S. H. Gellman, *J. Am. Chem. Soc.*, 1999, **121**, 4325-4333.
- 4 K. L. Geoghegan, P. J. Rosner and L. R. Hoth, *Bioconjugate Chem.*, 2000, **11**, 71-77.
- 5 M. Montalti, L. Prodi, E. Rampazzo and N. Zaccheroni, *Chem. Soc. Rev.*, 2014, **43**, 4243-4268.
- 6 X. Michalet, F. F. Pinaud, L. A. Bentolila, J. M. Tsay, S. Doose, J. J. Li, G. Sundaresan, A. M. Wu, S. S. Gambhir and S. Weiss, *Science*, 2005, **307**, 538-544.
- 7 M. K. So, C. Xu, A. M. Loening, S. S. Gambhir and J Rao, *Nat. Biotech.* 2006, **24**, 339-343.

- 8 B. Dubertret, P. Skourides, D. J. Noriis, V. Noireaux, A. H. Brivanlou and A. Libchader, *Science*, 2002, **298**, 1759-1762.
- 9 B. Ballou, B. C. Lagerholm, L. A. Ernst, M. P. Bruchez and A. S. Waggoner, *Bioconjugate Chem*, 2004, **15**, 79-86.
- 10 X. Liu and M. T. Swihart, *Chem. Soc. Rev.*, 2014, **43**, 3908-3920.
- 11 M. Bruchez, M. Moronne, P. Gin, S. Weiss and A. P. Alivisatos, *Science*, 1998, **281**, 2013-2016.
- 12 X. H. Huang, I. H. El-Sayed, W. Qian and M. A. El-Sayed, *J. Am. Chem. Soc.*, 2006, **128**, 2115-2120.
- 13 E. C. Dreaden, A. M. Alkilany, X. H. Huang, C. J. Murphy and M. A. El-Sayed, *Chem. Soc. Rev.*, 2012, **41**, 2740-2779.
- 14 P. D. Howes, S. Rana and M. M. Stevens, *Chem. Soc. Rev.*, 2014, **43**, 3835-3853.
- 15 S. Bhaumik and S. S. Gambhir, *Proc. Natl. Acad. Sci. USA*, 2002, **99**, 377-382.
- 16 C. H. Contag and M. H. Bachmann, *Annu. Rev. Biomed. Eng.*, 2002, **4**, 235-260.
- 17 Z. Cheng, J. Levi, Z. Xiong, O. Gheysens, S. Keren, X. Chen and S. S. Gambhir, *Bioconjugate Chem.*, 2006, **17**, 662-669.
- 18 R. Weissleder, C. H. Tung, U. Mahmood and A. Bogdanov, *Nat. Biotechnol.*, 1999, **17**, 375-378.
- 19 A. Becker, C. Hassenius, K. Licha, B. Ebert, U. Sukowski, W. Semmler, B. Wiedenmann and C. Grotzinger, *Nat. Biotechnol.*, 2001, **19**, 327-331.
- 20 G. Wagnieres, W. Star and B. Wilson, *Photochem. Photobiol.*, 1998, **68**, 603-632.
- 21 S. Andersson-Engels and B. Wilson, *J. Cell Pharmacol.*, 1992, **3**, 48-61.
- 22 F. Wang, D. Banerjee, Y. Liu, X. Chen and X. Liu, *Analyst*, 2010, **135**, 1839-1854.
- 23 G. Chen, J. Shen, T. Y. Ohulchanskyy, N. J. Patel, A. Kuikov, Z. Li, J. Song, R. K. Pandey, H. Agren and P. N. Prasad, *ACS Nano*, 2012, **6**, 8280-8287.
- 24 H. S. Mader, P. Kele, S. M. Saleh and O. S Wolfbeis, *Curr. Opin. Chem. Biol.*, 2010, **14**, 582-596.
- 25 M. Nyk, R. Kumar, T. Y. Ohulchanskyy, E. J. Bergey and P. N. Prasad, *Nano Lett.* 2008, **8**, 3834-3838.
- 26 G. Y. Chen, H. L. Qiu, P. N. Prasad and X. Y. Chen, *Chem. Rev.*, 2014, **114**, 5161-5214.
- 27 D. Yang, P. Ma, Z. Hou, Z. Cheng, C. Li and J. Lin, *Chem. Soc. Rev.* 2014, DOI: 10.1039/c4cs00155a.
- 28 F. Auzel, *Chem. Rev.*, 2004, **104**, 139-173.

- 29 R. V. Yadav, S. K. Singh, R. K. Verma and S. B. Rai, *Chem. Phys. Lett.*, 2014, **599**, 122-126.
- 30 S. K. Singh, A. K. Singh and S. B. Rai, *Nanotechnology*, 2011, **22**, 275703 (10 pages)
- 31 F. Wang, Y. Han, C. S. Lim, Y. H. Lu, J. Wang, J. Xu, H. Y. Chen, C. Zhang, M. H. Hong and X. G. Liu, *Nature*, 2010, **463**, 1061-1065.
- 32 S. K. Singh, K. Kumar and S. B. Rai, *Appl. Phys. B*, 2010, **100**, 443-446.
- 33 F. Wang and X. G. Liu, *Chem. Soc. Rev.*, 2009, **38**, 976-989.
- 34 S. K. Singh, K. Kumar and S. B. Rai, *Appl. Phys. B*, 2009, **94**, 165-173.
- 35 M. Pollnau, D. R. Gamelin, S. R. Luthi, H. U. Gudel and M. P. Hehlen, *Phys. Rev. B*, 2000, **61**, 3337-3346.
- 36 R. Weissleder, *Nat. Biotechnol.*, 2001, **19**, 316-317.
- 37 A. N. Bashkatov, E. A. Genina, V. I. Kochubey and V. V. Tuchin, *J. Phys. D: Appl. Phys.*, 2005, **38**, 2543-2555.
- 38 K. Welsher, S. P. Sherlock and H. J. Dai, *Proc. Natl. Acad. Sci. U. S. A.*, 2011, **108**, 8943-8948.
- 39 S. Heer, K. Kompe, H. U. Gudell and M. Haase, *Adv. Mater.*, 2004, **16**, 2102-2105.
- 40 Q. le Masne de Chermont, C. Chanéac, J. Seguin, F. Pellé, S. Maîtrejean, J. P. Jolivet, D. Gourier, M. Bessodes and D. Scherman, *Proc. Nat. Acad. Sci. USA*, 2007, **104**, 9266-9271.
- 41 Y. Li, S. Zhou, G. Dong, M. Peng, L. Wondraczek and J. Qiu, *Sci. Report*, 2014, **4**, 4059 (6 pages)
- 42 A. M. Smith, M. C. Mancini and S. Nie, *Nat. Nanotechnol.*, 2009, **4**, 710-711.
- 43 J. V. Frangioni, *Curr. Opin. Chem. Biol.*, 2003, **7**, 626-634.
- 44 K. Van den Eeckhout, D. Poelman and P. F. Smet, *Materials*, 2013, **6**, 2789-2818.
- 45 T. Ishigaki, A. Torisaka, K. Nomizu, P. Madhusudan, K. U. K. Todaa and M. Satoa, *Dalton Trans.*, 2013, **42**, 4781-4785.
- 46 H. F. Brito, J. Hölsä, T. Laamanen, M. Lastusaari, M. Malkamäki and L. C. V. Rodrigues, *Opt. Mater. Expr.*, 2012, **2**, 371-381.
- 47 Phosphor Handbook, ed. W. M. Yen, S. Shionoya and H. Yamamoto, CRC Press, Boca Raton, FL, USA, 2<sup>nd</sup> ed., 2007.
- 48 V. Sharma, A. Das, V. Kumar, O. M. Ntwaeaborwa and H. C. Swart, *J. Mater. Sci.*, 2014, **49**, 2225-2234.
- 49 W. He, T. Sh. Atabaev, H. K. Kim and Y. H. Hwang, *J. Phys. Chem. C*, 2013, **117**, 17894-17900.

- 50 Y. Li, S. Zhou, Y. Li, K. Sharafudeen, Z. Ma, G. Dong, M. Peng and J. Qiu, *J. Mater. Chem. C*, 2014, **2**, 2657-2663.
- 51 A. Abdulkayum, C. X. Yang, Q. Zhao, J. T. Chen, Lu-X. Dong and X. P. Yan, *Analy. Chem.*, 2014, **86**, 4096-4101.
- 52 M. Nazarov, Nor N. Awang, A. F. Mohd Noor and P. Ivannikov, *Microsc. Analy.* 2013, **27**, 13-16.
- 53 F. G. Martína, F. F. Martineza, P. Díaza, C. Colónb and A. A. Medinab, *J. Alloy. Comp.*, 2010, **501**, 193-197.
- 54 X. Li, F. Zhang and D. Zhao, *Chem. Soc. Rev.* 2014, DOI: 10.1039/c4cs00163J.
- 55 J. Zhang, Y. Li, X. Hao, Q. Zhang, K. Yang, L. Li, L. Ma, S. wang and X. Li, *Mini Rev. Med. Chem.*, 2011, **11**, 678-694.
- 56 T. Matsuzawa, Y. Aoki, N. Takeuchi and Y. Murayama, *J. Electrochem. Soc.*, 1996, **143**, 2670-2673.
- 57 P. Dorenbos, *J. Electrochem. Soc.*, 2005, **152**, H107-H110.
- 58 F. Clabau, X. Rocquefelte, S. Jobic, P. Deniard, M. H. Whangbo, A. Garcia, and T. Le Mercier, *Chem. Mater.*, 2005, **17**, 3904-3912.
- 59 T. Aitasalo, J. Holsa, H. Jungner, M. Lastusaari and J. Niittykoski, *J. Phys. Chem. B*, 2006, **110**, 4589-4598.
- 60 K. Van den Eeckhout, P. F. Smet and D. Poelman, *Materials*, 2010, **3**, 2536-2566.
- 61 Y. Zhuang, Y. Katayama, J. Ueda and S. Tanabe, *Opt. Mater.*, 2014, <http://dx.doi.org/10.1016/j.optmat.2014.05.035>
- 62 P. K. Ghosh and B. Ray, *Prog. Cryst. Growth Charact.*, 1992, **25**, 1-37.
- 63 Phosphor Handbook, ed. S. Shionoya and W. M. Yen, CRC Press, Boca Raton, FL, USA, 1<sup>st</sup> ed., 1998.
- 64 D. Jia, J. Zhu and B. Wu, *J. Electrochem. Soc.*, 2000, **147**, 386-389.
- 65 D. Jia, J. Zhu and B. Wu, *J. Electrochem. Soc.*, 2000, **147**, 3948-3952.
- 66 Y. Kojima, K. Aoyagi and T. Yasue, *J. Lumin.* 2005, **115**, 13-18.
- 67 Y. Hu, W. Zhuang, H. Ye, S. Zhang, Y. Fang and X. Huang, *J. Lumin.*, 2005, **111**, 139-145.
- 68 D. Xiaoxia, H. Shihua, Y. Fangtian and K. Kai, *J. Rare Earths*, 2009, **27**, 43-46.
- 69 Y. Kojima, K. Aoyagi and T. Yasue, *J. Lumin.*, 2007, **126**, 319-322.
- 70 Y. Kojima and T. Toyama, *J. Alloys Compd.*, 2009, **475**, 524-528.
- 71 S. S. Pitale, S. K. Sharma, R. N. Dubey, M. S. Qureshi and M. M. Malik, *Opt. Mater.*, 2009, **31**, 923-930.

- 72 S. Jiayue, L. Zhenxing and D. Haiyan, *J. Rare Earths*, 2011, **29**, 101-103.
- 73 L. Wenyu, L. Yingliang, A. Pengfei and C. Xiaobo, *J. Rare Earths*, 2009, **27**, 895-899.
- 74 D. C. R. Burbano, E. M. Rodriguez, P. Dorenbos, M. Bettinelli and J. A. Capobianco, *J. Mater. Chem. C*, 2014, **2**, 228-231.
- 75 X. Wang, Z. Zhang, Z. Tang and Y. Lin, *Mater. Chem. Phys.*, 2003, **80**, 1-5.
- 76 P. F. Ai, U. L. Liu, W. Y. Li and L. Y. Xiao, *Phys. B*, 2010, **405**, 3360-3364.
- 77 P. Zhang, Z. Hong, M. Wang, X. Fang, G. Qian and Z. Wang, *J. Lumin.*, 2005, **113**, 89-93.
- 78 B. Lei, Y. Liu, G. Tang, Z. Ye and C. Shi, *Mater. Chem. Phys.*, 2004, **87**, 227-232.
- 79 C. C. Kang, Ru-S. Liu, J. C. Chang and B. J. Lee, *Chem. Mater.*, 2003, **15**, 3966-3968.
- 80 J. Zhang, Y. Liu and S. Man, *J. Lumin.*, 2006, **117**, 141-146.
- 81 X. J. Wang, D. Jia and W. M. Yen, *J. Lumin.*, 2003, **102**, 34-37.
- 82 L. Lin, C. Shi, Z. Wang, W. Zhang and M. Yin, *J. Alloys Compd.* 2008, **466**, 546-550.
- 83 C. M. Abreu, R. S. Silva, M. E. G. Valerio and Z. S. Macedo, *J. Solid State Chem.* 2013, **200**, 54-59.
- 84 A. Bessière, A. Lecointre, K. R. Priolkar, D. Gouriera, *J. Mater. Chem.* 2012, **22**, 19039-19046.
- 85 A. Lecointre, A. Bessière, K. R. Priolkar, D. Gourier, G. Wallez and B. Viana, *Mater. Res. Bull.*, 2013, **48**, 1898-1905.
- 86 A. Lecointre, A. Bessière, B. Viana and D. Gourier, *Radiat. Meas.*, 2010, **45**, 497-499.
- 87 Z. He, X. -J. Wang and W. M. Yen, *J. Lumin.* 2007, **122-123**, 381-384.
- 88 Y. Gong, Y. Wang, X. Xu, Y. Li, S. Xin and L. Shi, *Opt. Mater.*, 2011, **33**, 1781-1785.
- 89 Y. Lin, Z. Zhang, Z. Tang, X. Wang, J. Zhang and Z. Zheng, *J. Euro. Ceram. Soc.*, 2001, **21**, 683-685.
- 90 Y. Gong, X. Xu, W. Zeng, C. Wu and Y. Wang, *Phys. Procedia*, 2012, **29**, 86-90.
- 91 Y. Cong, B. Li, S. Yue, L. Zhang, W. Li and X.-J. Wang, *J. Electrochem. Soc.*, 2009, **156**, H272-275.
- 92 Y. Katayama, J. Ueda and S. Tanabe, *Opt. Mater. Express*, 2014, **4**, 613-623.
- 93 P. F. Smet, K. Van der Eeckhout, A. J. J. Bos, E. van der Kolk and P. Drenbos, *J. Lumin.*, 2012, **132**, 682-689.
- 94 X. Xu, Y. Gong, W. Zeng and Y. Wang, *Phys. Procedia*, 2012, **29**, 62-64.
- 95 J. Wang, S. Wang and Q. Su, *J. Solid State Chem.*, 2004, **177**, 895-900.
- 96 J. Wang, S. Wang and Q. Su, *J. Mater. Chem.*, 2004, **14**, 2569-2574.

- 97 Y. -H. Song, H. -F. Zou, S. -C. Gan, Y. -F. Deng, G. -Y. Hong and J. Meng, *J. Mater. Sci.*, 2007, **42**, 4899-4904.
- 98 J. Wang, Q. Su and S. Wang, *Mater. Res. Bull.*, 2005, **40**, 590-598.
- 99 A. Lecointre, A. Bessiere, A. J. J. Bos, P. Dorenbos, B. Viana and S. Jacquart, *J. Phys. Chem. C*, 2011, **115**, 4217-4227.
- 100 A. Lecointre, R. A. Benhamou, A. Bessière, G. Wallez, M. Elaati and B. Viana, *Opt. Mater.*, 2011, **34**, 376-380.
- 101 A. Bessiere, A. Lecointre, R. A. Benhamou, E. Suard, G. Walleza and B. Viana, *J. Mater. Chem. C*, 2013, **1**, 1252-1259.
- 102 A. Bessière, R. A. Benhamou, G. Wallez, A. Lecointre and B. Viana, *Acta Mater.*, 2012, **60**, 6641-6649.
- 103 H. Hosono, T. Kinoshita, H. Kawazoe, M. Yamazaki, Y. Yamamoto and N. Sawanobori, *J. Phys. Cond. Matt.*, 1998, **10**, 9541-9547.
- 104 W. Jia, D. Jia, T. Rodriguez, D. R. Evans, R. S. Meltzer and W. M. Yen, *J. Lumin.*, 2006, **119/120**, 13-18.
- 105 S. Lian, Y. Qi, C. Rong, L. Yu, A. Zhu, D. Yin and S. Liu, *J. Phys. Chem. C*, 2010, **114**, 7196-7204.
- 106 J. Fu, *Electrochem. Solid State Lett.*, 2000, **3**, 350-351.
- 107 A. Wiatrowska and E. Zych, *J. Phys. Chem. C*, 2013, **117**, 11449-11458.
- 108 V. K. Jain, *Radiat. Phys. Chem.*, 1990, **36**, 47-57.
- 109 T. Maldiney, G. Sraiki, B. Viana, D. Gourier, C. Richard, D. Scherman, M. Bessodes, K. Van den Eeckhout, D. Poelman and P. F. Smet, *Opt. Mater. Expr.* 2012, **2**, 261-268.
- 110 D. Naczynski, M. Tan, M. Zevon, B. Wall, J. Kohl, A. Kulesa, S. Chen, C. Roth, R. Riman and P. Moghe, *Nat. Commun.*, 2013, **4**, 2199 (10 pages)
- 111 S. Nioka, S. Wen, J. Zhang, J. Du, X. Intes, Z. Zhao and B. Chance, Oxygen Transport to Tissue XXVI, ed P. Okunieff, J. Williams and Y. Chen, Springer, New York, 2005, vol. 566, ch. 3, pp. 17-22.
- 112 R. Wang and F. Zhang, *J. Mater. Chem. B*, 2014, **2**, 2422-2443.
- 113 J. C. G. Bünzli and S. V. Eliseeva, *J. Rare Earths*, 2010, **28**, 824-842.
- 114 S. Comby and J. C. G. Bünzli, Handbook on the Physics and Chemistry of Rare Earths., ed. K. A. Jr Gschneidner, J-C G Bünzli and V. K. Pecharsky, Elsevier Science B.V., Amsterdam, 2007, vol. 37, ch. 235, pp. 217-470.
- 115 J. Ueda, T. Shinoda and S. Tanabe, *Opt. Mater. Expr.* 2013, **3**, 787-793.

- 116 Y. Teng, J. Zhou, Z. Ma, M. M. Smedskjaer and J. Qiu, *J. Electrochem. Soc.* 2011, **158**, K17-K19.
- 117 N. Yu, F. Liu, X. Li and Z. Pan, *Appl. Phys. Lett.* 2009, **95**, 231110 (3 pages)
- 118 Y. Tanabe and S. Sugano, *J. Phys. Soc. Japan*, 1954, **9**, 753-766.
- 119 Y. Tanabe and S. Sugano, *J. Phys. Soc. Japan*, 1954, **9**, 766-779.
- 120 Y. Tanabe and S. Sugano, *J. Phys. Soc. Japan*, 1956, **11**, 864-877.
- 121 G. Blasse and B. C. Grabmaier. *Luminescent Materials*. Springer Verlag, Berlin Heidelberg, 1994.
- 122 B. Henderson and G. F. Imbusch. *Optical Spectroscopy of Inorganic Solids*, Clarendon Press, Oxford, 1989.
- 123 T. Maldiney, C. Richard, J. Seguin, N. Wattier, M. Bessodes and D Scherman, *ACS Nano*, 2011, **5**, 854-862.
- 124 T. Maldiney, M. U. Kaikkonen, J. Seguin, Q. le Masne de Chermont, M. Bessodes, K. J. Airene, S. Y. Herttuala, D. Scherman and C. Richard, *Bioconj. Chem.*, 2012, **23**, 472-478.
- 125 T. Maldiney, G. Byk, N. Wattier, J. Seguin, R. Khandadash, M. Bessodes, C. Richard and D. Scherman, *Intern. J. Pharmac.*, 2012, **423**, 102-107.
- 126 T. Maldiney, A. Lecointre, B. Viana, A. Bessiere, M. Bessodes, D. Gourier, C. Richard and D. Scherman, *J. Am. Chem. Soc.* 2011, **133**, 11810-11815.
- 127 Z. J. Li, J. Shi, H. Zhang and M. Sun, *Opt. Express*, 2014, **22**, 10509-10518.
- 128 R. Pang, Y. Jia, R. Zhao, H. Li, J. Fu, W. Sun, L. Jiang, Su Zhang, C. Li and Q. Su. *Dalton Trans.*, 2014, **43**, 9661-9668.
- 129 Y. Li, Yi-Y. Li, K. Sharafudeen, G. P. Dong, S. F. Zhou, Z. J. Ma, M. Y. Peng and J. R. Qiu, *J. Mater. Chem. C*, 2014, **2**, 2019-2027.
- 130 A. Bessière, S. Jacquart, K. Priolkar, A. Lecointre, B. Viana, D. Gourier, *Opt. Express*, 2011, **19**, 10131-10137.
- 131 Y. Zhuang, J. Ueda and S. Tanabe, *Appl. Phys. Express*, 2013, **6**, 052602 (4 pages)
- 132 A. Bessière, S. K. Sharma, N. Basavaraju, K. R. Priolkar, L. Binet, B. Viana, A. J. J. Bos, T. Maldiney, C. Richard, D. Scherman and D. Gourier, *Chem. Mater.*, 2014, **26**, 1365-1373.
- 133 Y. Zhuang, J. Ueda, S. Tanabe and P. Dorenbos, *J. Mater. Chem. C*, 2014, **2**, 5502-5509.

- 134 T. Maldiney, A. Bessière, J. Seguin, E. Teston, S. K. Sharma, B. Viana, A. J. J. Bos, P. Dorenbos, M. Bessodes, D. Gourier, D. Scherman and C. Richard, *Nat. Mater.*, 2014, **13**, 418-426.
- 135 D. Gourier, A. Bessière, S. K. Sharma, L. Binet, B. Viana, N. Basavaraju and K. R. Priolkar, *J. Phys. Chem. Sol.*, 2014, **75**, 826-837.
- 136 S. K. Sharma, A. Bessière, N. Basavaraju, K. R. Priolkar, L. Binet, B. Viana and D. Gourier, *J. Lumin.*, 2014, **155**, 251-256.
- 137 Z. Pan, Y. Lu and F. Liu, *Nat. Mater.*, 2012, **11**, 58-63.
- 138 A. Abdukayum, J. Chen, Q. Zhao and X. Yan, *J. Am. Chem. Soc.* 2013, **135**, 14125-14133.
- 139 M. Allix, S. Chenu, E. Véron, T. Poumeyrol, E. Kouadri-Boudjelthia, S. Alahraché, F. Porcher, D. Massiot and F. Fayon, *Chem. Mater.*, 2013, **25**, 1600-1606.
- 140 Y. Zhuang, J. Ueda and S. Tanabe, *J. Mater. Chem. C*, 2013, **1**, 7849-7855.
- 141 F. Liu, W. Yan, Y. Chuang, Z. Zhen, J. Xie and Z. Pan, *Sci. Rep.*, 2013, **3**, 1554 (9 pages).
- 142 X. Fu, C. Liu, J. Shi, H. Mana, J. Xu and H. Zhang, *Opt. Mater.*, 2014 <http://dx.doi.org/10.1016/j.optmat.2014.04.018>
- 143 D. Chen, *J. Eur. Ceram. Soc.*, 2014, **35**, 4069-4075.
- 144 Y. Lu, F. Liu, Z. Gu and Z. Pan, *J. Lumin.*, 2011, **131**, 2784-2787.
- 145 X. Wang, M. Wan, Y. Wang, H. Zhao, Z. Hu and H. Li, *Spectrosc. Spectr. Anal.*, 2013, **33**, 2921-2925.
- 146 N. Basavaraju, S. Sharma, A. Bessière, B. Viana, D. Gourier and K. Priolkar, *J. Phys. D: Appl. Phys.*, 2013, **46**, 375401 (5 pages)
- 147 W. Zhang, Y. Wang, H. Li, X. Wang and H. Zhao, *Spectrosc. Spectr. Anal.*, 2013, **33**, 31-35.
- 148 J. Xu, D. Chen, Y. Yu, W. Zhu, J. Zhou and Y. Wang, *Chem. Asian J.*, 2014, **9**, 1020-1025.
- 149 G. Blasse, B. C. Grabmaier and M. Ostertag, *J. Alloys Compd.* 1993, **200**, 17-18.
- 150 L. Kostyk, A. Luchechko, Ya. Zakharko, O. Tsvetkova and B. Kuklinski, *J. Lumin.*, 2009, **129**, 312-316.
- 151 J. Ueda, K. Kuroishi and S. Tanabe, *Appl. Phys. Lett.* 2014, **104**, 101904 (3 pages).
- 152 W. Yan, F. Liu, Y. Lu, X. Wang, M. Yin and Z. Pan, *Opt. Express*, 2010, **18**, 20215-20221.
- 153 D. Jia, L. Lewis and X. Wang, *Electrochem. Solid State Lett.*, 2010, **13**, J32-J34.

- 154 H. N. Luitel, T. Watari, T. Torikai and M. Yada, *Opt. Mater.* 2009, **31**, 1200-1204
- 155 H. E. Swanson, R. K. Fuyat and G. M. Ugrinie, *Nat. Bur. Stand. (U.S.) Cric.*, 1955, No. **539 IV**, 25.
- 156 S. J. Geller, *J. Chem. Phys.*, 1960, **33**, 676-684.
- 157 K. Pohl, *Naturwissenschaften*, 1968, **55**, 82.
- 158 S. J. Schneider and J. L. Waring, *J. Res. Nat. Bur. Stand.*, 1963, **A67**, 19.
- 159 D. Errandonea, R. Kumar, F. Manjón, V. Ursaki and E. Rusu, *Phys. Rev. B*, 2009, **79**, 024103 (6 pages).
- 160 M. Allix, S. Chenu, E. Ve, T. Poumeyrol, E. A. Kouadri-boudjelthia, S. Alahrache, F. Porcher and D. Massiot, *Chem. Mater.*, 2013, **25**, 1600-1606.
- 161 L. H. Reddy, J. L. Arias, J. Nicolas and P. Couvreur, *Chem. Rev.*, 2012, **112**, 5818-5878.
- 162 M. Colombo, S. Carregal-Romero, M. F. Casula, L. Gutierrez, M. P. Morales, I. B. Bohm, J. T. Heverhagen, D. Prospero and W. Parak, *J. Chem. Soc. Rev.* 2012, **41**, 4306-4334.
- 163 D. Chen, Y. Chen, H. Lu and Z. Ji, *Inorg. Chem.* 2014, **53**, 8638-8645.

**Table 1:** Detail of host matrix, dopant ion(s), emission colour/wavelength, and duration of persistent luminescence of different types of red emitting persistent materials.

Host <sup>Reference</sup>	Dopant ion(s)	$\lambda_{\text{Emission}}$ (nm)	Persistent time	Remarks
CaS <sup>64</sup>	Eu <sup>2+</sup> , Tm <sup>3+</sup> / Bi <sup>3+</sup>	650	1h	Effect of Na <sup>+</sup> co-doping
CaS <sup>65</sup>	Eu <sup>2+</sup>	655/670	--	Effect of Cl <sup>-</sup> co-doping
CaS <sup>66</sup>	Bi <sup>3+</sup>	650	1h	Effect of Cl <sup>-</sup> co-doping
CaS <sup>67</sup>	Ce <sup>3+</sup> , Pr <sup>3+</sup>	Green/red	1h	Effect of Li <sup>+</sup> co-doping
Ca <sub>1-x</sub> Sr <sub>x</sub> S <sup>68</sup>	Eu <sup>2+</sup>	650	1h	White light emission
SrS <sup>69</sup>	Eu <sup>2+</sup> , Dy <sup>3+</sup>	616	--	Nano-size particle
CaS <sup>70</sup>	Eu <sup>2+</sup> , Pr <sup>3+</sup>	--	--	Effect of Li <sup>+</sup> co-doping
Ca <sub>1-x</sub> Sr <sub>x</sub> S <sup>71</sup>	Eu <sup>2+</sup> , Pr <sup>3+</sup>	650	--	Effect of Li <sup>+</sup> co-doping
SrS <sup>72</sup>	Pr <sup>3+</sup>	Blue/green/red	--	--
SrS <sup>73</sup>	Eu <sup>2+</sup>	615	--	Lanthanide(3+) co-doping
CaS <sup>74</sup>	Eu <sup>2+</sup> , Dy <sup>3+</sup>	650	--	Nano, photostimulated
Y <sub>2</sub> O <sub>2</sub> S <sup>75</sup>	Eu <sup>3+</sup> , Mg <sup>2+</sup> , Ti <sup>4+</sup>	611	1h	Nanorods
Y <sub>2</sub> O <sub>2</sub> S <sup>76</sup>	Eu <sup>3+</sup> , Mg <sup>2+</sup> , Ti <sup>4+</sup>	611	1h	Solid state reaction
Y <sub>2</sub> O <sub>2</sub> S <sup>77</sup>	Ti <sup>4+</sup> /Ti <sup>2+</sup>	565	5h	High temp sintering
Y <sub>2</sub> O <sub>2</sub> S <sup>78</sup>	Sm <sup>3+</sup>	610	1h	--
Y <sub>2</sub> O <sub>2</sub> S <sup>79</sup>	Mg <sup>2+</sup> , Ti <sup>4+</sup>	594, broad	--	High Temperature
Gd <sub>2</sub> O <sub>2</sub> S <sup>80</sup>	Er <sup>3+</sup> /Ti <sup>4+</sup>	555, 675	1.2	--
MgSiO <sub>3</sub> <sup>81, 82</sup>	Mn <sup>2+</sup> , Eu <sup>2+</sup> , Dy <sup>3+</sup>	660	4h	High temp sintering
CdSiO <sub>3</sub> <sup>83</sup>	Mn, Ni, Cr	550-720	<1	Solid state reaction
CaMgSi <sub>2</sub> O <sub>6</sub> <sup>84, 85</sup>	Mn	550-800	<1	Sol-gel route
CaMgSi <sub>2</sub> O <sub>6</sub> <sup>86</sup>	Mn <sup>2+</sup> , Dy <sup>3+</sup>	550-800	<1	Nanoparticle synthesis
SrMg(SiO <sub>3</sub> ) <sub>2</sub> <sup>87</sup>	Mn <sup>2+</sup> , Dy <sup>3+</sup>	500-800	<1	Solid state reaction
Sr <sub>3</sub> MgSi <sub>2</sub> O <sub>8</sub> <sup>88</sup>	Eu <sup>2+</sup> , Mn <sup>2+</sup> , Dy <sup>3+</sup>	670	2h	Solid state reaction
BaMg <sub>2</sub> Si <sub>2</sub> O <sub>7</sub> <sup>89</sup>	Mn <sup>2+</sup> , Ce <sup>3+</sup>	620/670	2h	Solid phase reaction
Ca <sub>3</sub> MgSi <sub>2</sub> O <sub>8</sub> <sup>90</sup>	Eu <sup>2+</sup> , Dy <sup>3+</sup>	Green/red	5h	--
MgGeO <sub>3</sub> <sup>91, 92</sup>	Yb <sup>3+</sup> /Bi <sub>2</sub> O <sub>3</sub>	600-720	--	-
M <sub>2</sub> Si <sub>5</sub> N <sub>8</sub> <sup>93</sup>	Eu (M=Ca, Sr, Ba)	580-620	--	--
Ca <sub>2</sub> SnO <sub>4</sub> <sup>94</sup>	Sm <sup>3+</sup>	Orange-red	--	--
$\beta$ -Zn <sub>3</sub> (PO <sub>4</sub> ) <sub>2</sub> <sup>95</sup>	Mn <sup>2+</sup>	616	2h	Role of excess Zn <sup>2+</sup>
$\beta$ -Zn <sub>3</sub> (PO <sub>4</sub> ) <sub>2</sub> <sup>96, 97</sup>	Mn <sup>2+</sup> , Al <sup>3+</sup> , Ga <sup>3+</sup>	570-700	--	Solid state reaction
$\beta$ -Zn <sub>3</sub> (PO <sub>4</sub> ) <sub>2</sub> <sup>98</sup>	Sm <sup>3+</sup> , Mn <sup>2+</sup>	616	2h	Solid state reaction
YPO <sub>4</sub> <sup>99</sup>	Pr <sup>3+</sup> , Ln <sup>3+</sup>	Red	--	High temperature
Ca <sub>3</sub> (PO <sub>4</sub> ) <sub>2</sub> <sup>100, 101</sup>	Mn <sup>2+</sup> /Tb/Dy	660	--	Biocompatible host
Ca <sub>9</sub> Ln(PO <sub>4</sub> ) <sub>7</sub> <sup>102</sup>	Lanthanides, Mn	Red	--	--
CaO-Al <sub>2</sub> O <sub>3</sub> <sup>103</sup>	Tb <sup>3+</sup>	Green/red	--	Glass
CaTiO <sub>3</sub> <sup>104</sup>	Pr <sup>3+</sup>	612	0.1	--
CaTiO <sub>3</sub> <sup>104</sup>	Al <sup>3+</sup>	612	0.2	--
Ca <sub>2</sub> Zn <sub>4</sub> Ti <sub>16</sub> O <sub>38</sub> <sup>105</sup>	Pr <sup>3+</sup>	614, 644	--	Dual phosphorescence
MO <sup>106</sup>	Eu (M=Ca, Sr, Ba)	Orange-red	2h	Solid state reaction
Lu <sub>2</sub> O <sub>3</sub> <sup>107</sup>	Pr, Hf	610, 632	--	Thermal/photostimulation
CaF <sub>2</sub> <sup>108</sup>	Tm/Dy/Mn	Miscellaneous	--	--
Ca <sub>2</sub> Si <sub>5</sub> N <sub>8</sub> <sup>109</sup>	Eu <sup>2+</sup> , Tm <sup>3+</sup>	610	--	Bioimaging application

**Table 2:** Detail of host, co-dopant ion(s), emission wavelength, *etc* of NIR persistent materials activated with Mn<sup>2+</sup> ions.

Host <sup>References</sup>	Co-dopants	$\lambda_{\text{emission}}$	Remarks
Ca <sub>0.2</sub> Zn <sub>0.9</sub> Mg <sub>0.9</sub> Si <sub>2</sub> O <sub>6</sub> <sup>40</sup>	Eu <sup>2+</sup> , Dy <sup>3+</sup>	699 nm	Persistent time more than 24 h, Surface functionalization with PEG and amino groups, imaging and tumour targeting applications
Ca <sub>0.2</sub> Zn <sub>0.9</sub> Mg <sub>0.9</sub> Si <sub>2</sub> O <sub>6</sub> <sup>123</sup>	Eu <sup>2+</sup> , Dy <sup>3+</sup>	699 nm	Surface functionalization with Methoxy-PEG of different molecular weight, Cancer imaging
Ca <sub>0.2</sub> Zn <sub>0.9</sub> Mg <sub>0.9</sub> Si <sub>2</sub> O <sub>6</sub> <sup>124</sup>	Eu <sup>2+</sup> , Dy <sup>3+</sup>	699 nm	Biotinylated PEG-PLNPs, Protein binding and avidin expressing glioma cells targeting application
Ca <sub>0.2</sub> Zn <sub>0.9</sub> Mg <sub>0.9</sub> Si <sub>2</sub> O <sub>6</sub> <sup>125</sup>	Eu <sup>2+</sup> , Dy <sup>3+</sup>	699 nm	Functionalization with Rak-2, Prostate cancer cells imaging application
CaMgSi <sub>2</sub> O <sub>6</sub> <sup>126</sup>	Eu <sup>2+</sup> , Ln <sup>3+</sup>	685 nm	Eu, Pr, Mn co-doping yield best results
SiO <sub>2</sub> /CaMgSi <sub>2</sub> O <sub>6</sub> <sup>127</sup>	(Ln=Dy, Pr, Ce, Nd) Eu <sup>2+</sup> , Pr <sup>3+</sup>	660 nm	bioimaging application
Zn <sub>2</sub> P <sub>2</sub> O <sub>7</sub> <sup>128</sup>	Tm <sup>3+</sup>	690 nm	Biocompatible, Imaging application
MAIO <sub>3</sub> <sup>129</sup>	Mn <sup>4+</sup> /Ge <sup>4+</sup> (M=La, Gd)	730 nm	Blue (Tm only), Red (Mn only) and NIR (Tm, Mn both) persistent luminescence Bioimaging in pork tissue

**Table 3:** Detail of host, emission wavelength, and duration of persistent luminescence (in h) of NIR persistent materials, *etc.* activated with Cr<sup>3+</sup> ions.

Host <sup>References</sup>	$\lambda_{\text{Emission}}$ (nm)	Time (h)	Remarks
ZnGa <sub>2</sub> O <sub>4</sub> <sup>130, 131, 136</sup>	650-730	>1	Solid state reaction, variation of Cr <sup>3+</sup> concentration
ZnGa <sub>2</sub> O <sub>4</sub> <sup>132, 133, 135</sup>	650-730	>1	Zn deficiency improves persistent luminescence
ZnGa <sub>2</sub> O <sub>4</sub> <sup>134</sup>	650-730	>1	Low temperature sintering, imaging of vascularization, tumours and grafted cells
Zn <sub>3</sub> Ga <sub>2</sub> Ge <sub>2</sub> O <sub>10</sub> <sup>137</sup>	650-1,000	>360	Solid state reaction, Sunlight activated, all weather material
Zn <sub>3</sub> Ga <sub>2</sub> Ge <sub>2</sub> O <sub>10</sub> <sup>41</sup>	630-750	>360	Photostimulation through incoherent light, Imaging of pork tissue, cytotoxicity
Zn <sub>3</sub> Ga <sub>2</sub> Sn <sub>1</sub> O <sub>8</sub> <sup>50</sup>	650-800	>300	Imaging in goldfish
Zn <sub>2.94</sub> Ga <sub>1.96</sub> Ge <sub>2</sub> O <sub>10</sub> <sup>138</sup>	650-800	>360	Pr <sup>3+</sup> co-dopant, Zn deficiency, surface functionalization with PEG and RGDyK
Zn <sub>1+x</sub> Ga <sub>2-2x</sub> (Ge/Sn) <sub>x</sub> O <sub>4</sub> <sup>139</sup>	640-780	>360	Replacement of Ga by Sn/Ge in ZnGa <sub>2</sub> O <sub>4</sub>
Zn(Ga <sub>1-x</sub> Al <sub>x</sub> ) <sub>2</sub> O <sub>4</sub> <sup>140</sup>	640-780	--	Replacement of Ga by Al in ZnGa <sub>2</sub> O <sub>4</sub> , Co-doping of Bi
LiGa <sub>5</sub> O <sub>8</sub> <sup>141</sup>	640-780	>1000	<i>In vivo</i> imaging, visible light stimulation
LiGa <sub>5</sub> O <sub>8</sub> <sup>142</sup>	640-780	--	Surface functionalization with PEG-OCH <sub>3</sub> , <i>in vivo</i> imaging
LiGa <sub>5</sub> O <sub>8</sub> <sup>143</sup>	640-780	---	Embedded in glass matrix
Ga <sub>2</sub> O <sub>3</sub> <sup>144</sup>	640-780	>1	Nanowire assemblies
Ga <sub>2</sub> O <sub>3</sub> <sup>145</sup>	600-800	<1	Co-doping with Zn <sup>2+</sup> , Photocatalytic activity
Mg/SrGa <sub>2</sub> O <sub>4</sub> <sup>146-148</sup>	630-780	--	New phosphors
Gd <sub>3</sub> Ga <sub>5</sub> O <sub>12</sub> <sup>149, 150</sup>	630-800	--	--
Y <sub>3</sub> Al <sub>2</sub> Ga <sub>3</sub> O <sub>10</sub> <sup>151</sup>	660-750	--	---
La <sub>3</sub> Ga <sub>5</sub> GeO <sub>14</sub> <sup>152, 153</sup>	600-1400	--	Excitation dependent emission
Sr <sub>4</sub> Al <sub>14</sub> O <sub>25</sub> <sup>154</sup>	680-850	<1	Eu <sup>2+</sup> and Dy <sup>3+</sup> as co-dopants

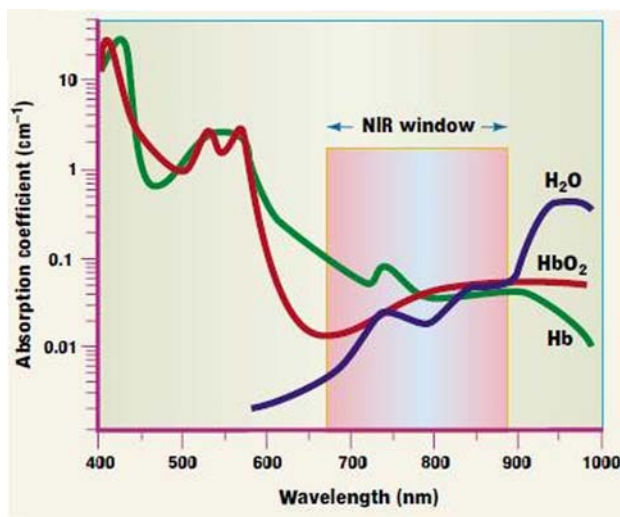


**Fig. 1** Absorption coefficient of haemoglobin and water in the 400–1000 nm range. Reprinted by permission from Macmillan Publishers Ltd: [Nature Biotechnology] (Ref 36), copyright (2001).

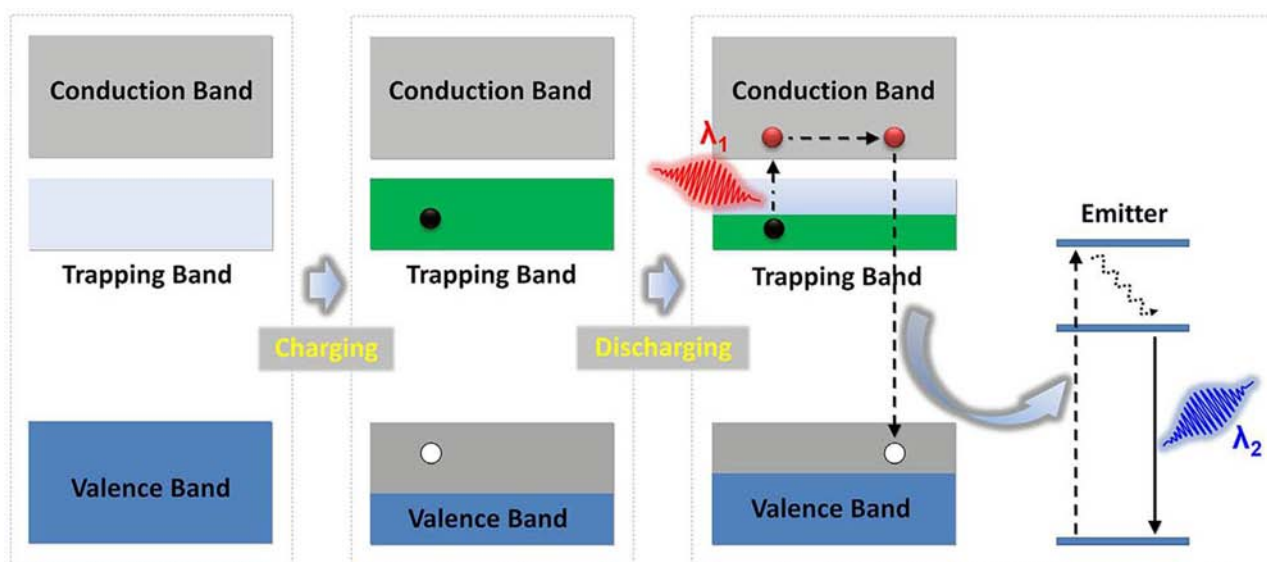


**Fig. 2:** Energy band model depicting anti-Stokes emission under incoherent excitation. During an optical charging process, the gap between valence and conduction band is decreased by generating an electron-hole pair. The trapped electron migrates into a satellite trapping band, from where it can be extracted by optical pumping. Emission of a secondary photon with lower wavelength than occurs through recombination of the electron-hole pair. Reproduced from Ref. 41.

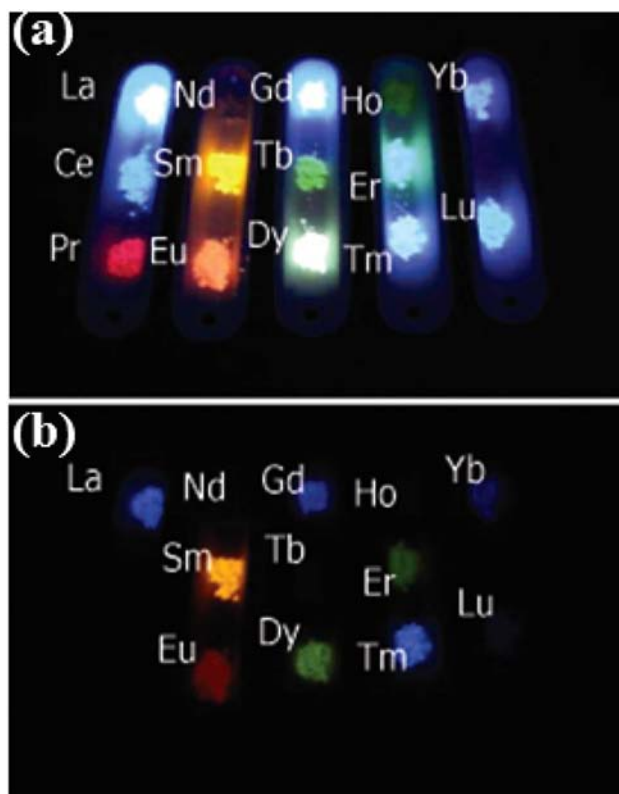


**Fig. 3:** Phosphorescence observation for La, Sm, Eu, Gd, Tb, Dy, Ho, Er, Tm, Yb, and Lu doped samples, (a) excited at 254 nm (photoluminescence), (b) after 5 seconds afterglow (emission). Reproduced from ref. 45 with permission from The Royal Society of Chemistry.

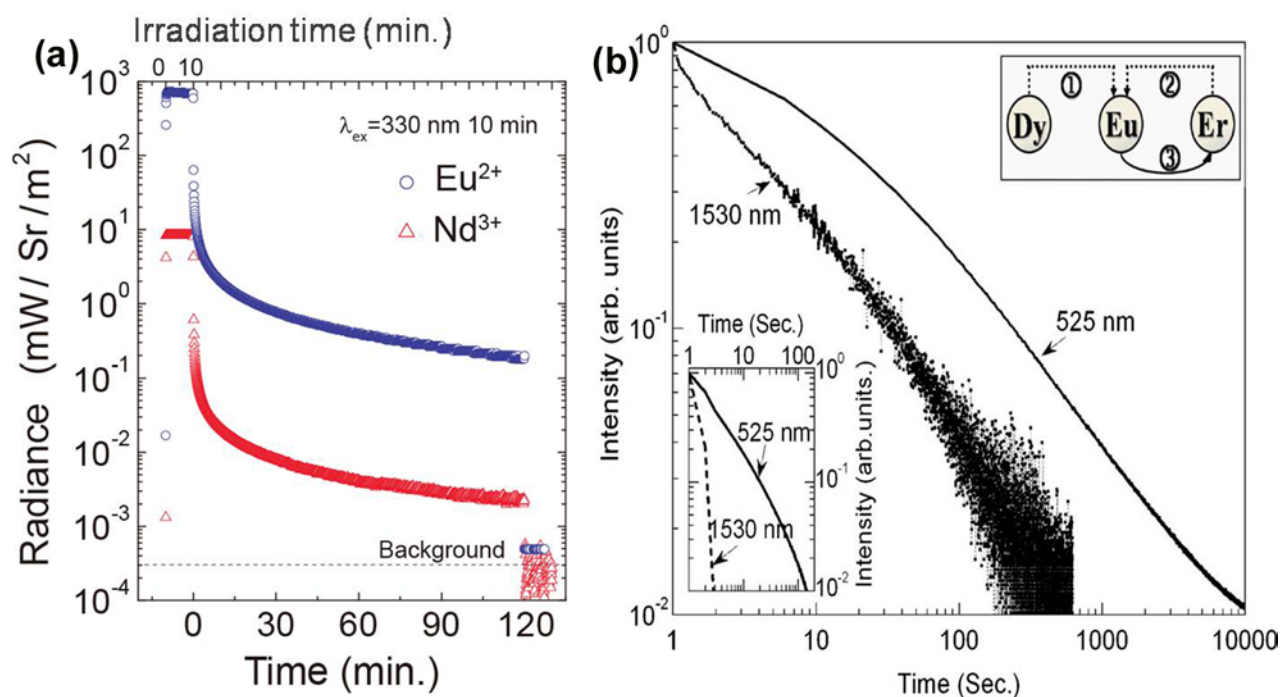


**Fig. 4** (a)-Afterglow curves for the persistent luminescence of  $\text{Eu}^{2+}$  and  $\text{Nd}^{3+}$  in  $\text{CaAl}_2\text{O}_4:\text{Eu}^{2+}-\text{Nd}^{3+}$  after 10 min of excitation by 330 nm light. (b)-Phosphorescence decay curves of  $\text{SrAl}_2\text{O}_4: 1.0\%\text{Eu}^{2+}, 1.5\%\text{Dy}^{3+},$  and  $2\%\text{Er}^{3+}$  phosphor for 525 and 1530 nm emissions. The upper right inset is the proposed charge trapping and energy transfer processes among Eu, Dy, and Er ions. The bottom left inset is the phosphorescence decay curves of  $\text{SrAl}_2\text{O}_4: 1.0\%\text{Eu}^{2+}, 2\%\text{Er}^{3+}$  phosphor for 525 and 1530 nm emissions. (a) Reprinted with permission from [Ref. 115]. Copyright [2013], Optical Society of America. (b) Reprinted with permission from [Ref. 117]. Copyright [2009], AIP Publishing LLC.

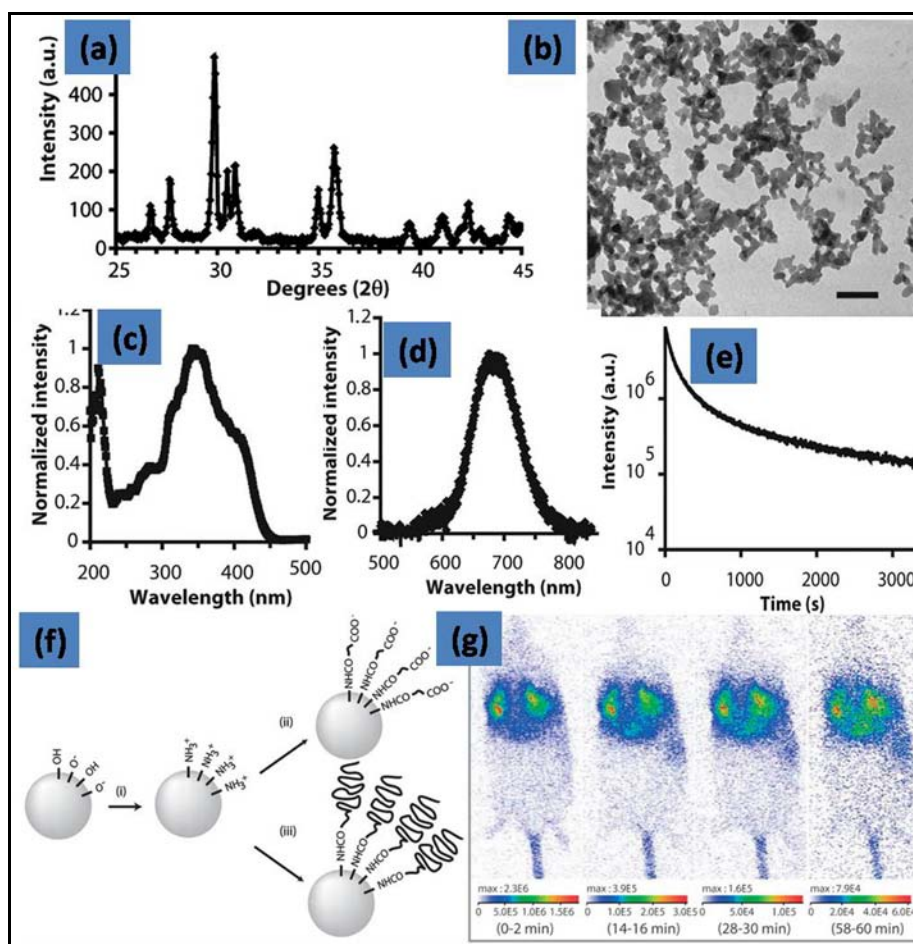


**Fig. 5** Physical characteristics of long afterglow  $\text{Ca}_{0.2}\text{Zn}_{0.9}\text{Mg}_{0.9}\text{Si}_2\text{O}_6$  nanoparticles, **(a)** XRD pattern showing clinoenstatite-like structure, **(b)** Transmission electron microscopy images (scale bar: 200 nm), **(c)** Excitation spectrum, **(d)** Long afterglow emission spectrum, **(e)** Time dependence of the luminescence intensity of the nanoparticles (NPs). NPs (10 mg) were put in 96-well plates under direct exposure to a 6 W UV lamp for 5 min. The luminous intensity was quantified straightforward by using an intensified charge-coupled device (ICCD) camera (Photon Imager; Biospace). Data analysis was performed by signal integration for 5 s. The luminous decay data were fit by a power law function for time 100 s. **(f)** Schematic representation of NP surface modification, (i) Amino-NPs, (ii) Carboxyl-NPs, (iii) PEG-NPs, and **(g)** Optical imaging of mouse with 1-mg tail vein injections of amino-NPs. Reproduced with permission from ref. 40, Copyright (2007) National Academy of Sciences, U.S.A.

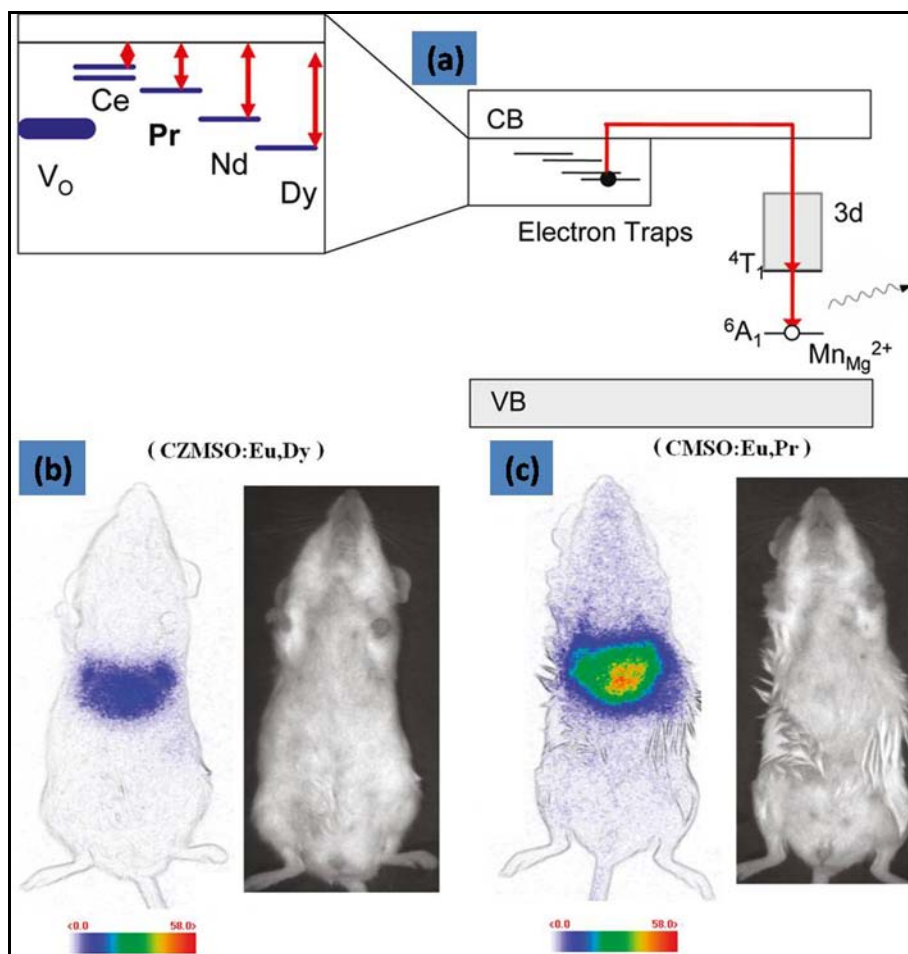


**Fig. 6** (a) Schematic energy level diagram of Mn<sup>2+</sup> and Ln<sup>3+</sup> in CaMgSi<sub>2</sub>O<sub>6</sub> (CMSO) host. The main hole traps are Mn<sup>2+</sup> ions in the Mg<sup>2+</sup> site, while electrons are trapped by oxygen vacancies (V<sub>O</sub>) and Ln<sup>3+</sup> ions. Thermally stimulated luminescence (TSL) and persistent luminescence occur by thermally activated electron release and capture by Mn<sup>3+</sup> ions, giving the Mn<sup>2+</sup> emission. The insert shows the relative positions of electron trap levels with respect to the conduction band edge. In vivo imaging of (b) Ca<sub>0.2</sub>Zn<sub>0.9</sub>Mg<sub>0.9</sub>Si<sub>2</sub>O<sub>6</sub> (CZMSO):Eu, Dy; and (c) CMSO:Eu, Pr PLNPs under the photon-counting system. The signal was recorded for 15 min following systemic injection of the probes (100 μg, excited 5 min under a 6W UV lamp at 254 nm before injection). Luminescence intensity is expressed in false color units (1 unit = 2800 photons per s.cm<sup>2</sup>.steradians). For both compositions (b and c), the left picture represents the luminescence signal from PLNP, and the right picture represents the photograph of the imaged mouse. Reprinted (adapted) with permission from Ref. 126. Copyright (2011) American Chemical Society.

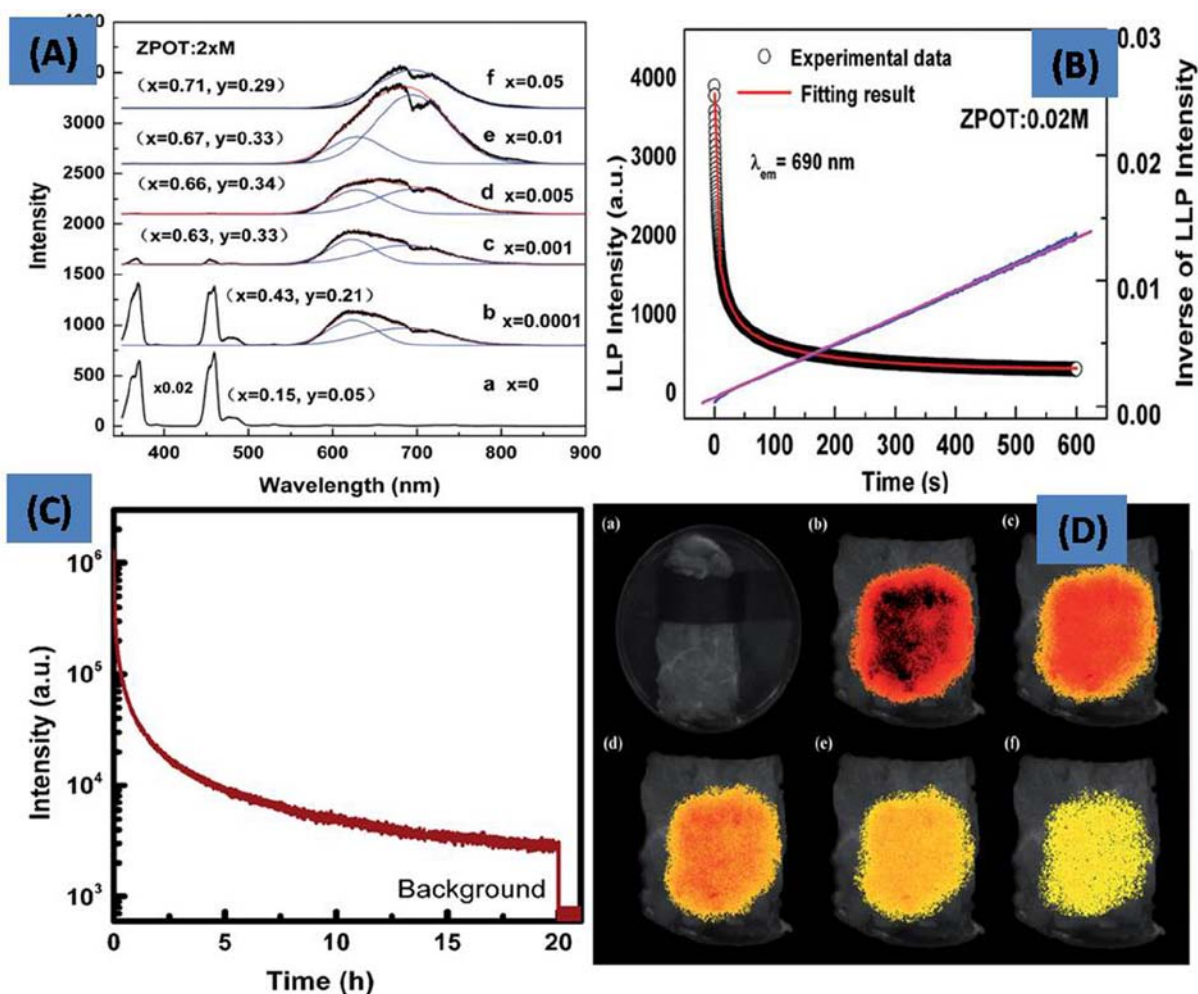


**Fig. 7** (A) The LLP emission spectra of ZPOT: 2xM ( $0 \leq x \leq 0.05$ ) measured at 5 min after ceasing the 254 nm excitation source, (B) LLP decay curves (black circle) and the plots of inverse of LLP intensity ( $I^{-1}$ ) versus time (t) (blue line) monitored at 690 nm for ZPOT: 0.02M, (C) Persistent luminescence properties of sample LAM21, afterglow intensity monitored at 731 nm as a function of time. The phosphor was pre-irradiated by a xenon lamp for 10 min, (D) Long persistent luminescence tissues imaging of pork tissue (a) Pre-injection image, and (b) 1, (c) 10, (d) 30, (e) 120, and (f) 720 min post-injection fluorescence images. The sample GAM23 was pre-excited at 325 nm for 10 min before the injection. Injection of sample (1g) mixing into normal saline (10 ml); injection depth was 3 mm under the epidermis. (a, b) Reproduced from ref. 128, (c, d) Reproduced from ref. 129 with permission from The Royal Society of Chemistry.

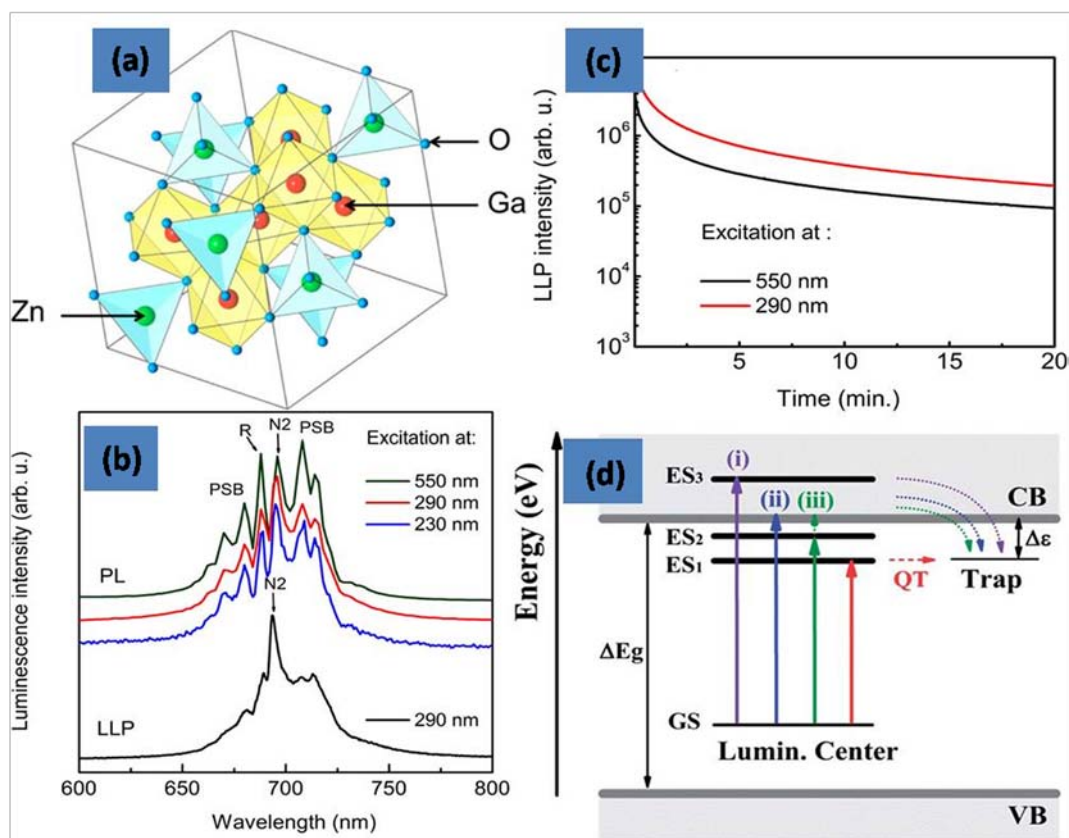


**Fig. 8** (a) Cubic spinel structure of ZnGa<sub>2</sub>O<sub>4</sub> (ZGO); (b) Normalized PL spectra of ZGO:Cr and LLP emission spectrum at RT, 10 s after the end of a 290 nm excitation; (c) LLP decays measured after a 15 min laser excitation at 550 nm (11 mJ) and 290 nm (3 mJ); (d) Schematic energy level diagram showing typical electron trapping processes. CB and VB refer to the conduction band and the valence band of the host; GS and ES are the ground state and excited state of the luminescent center. Arrows (i), (ii), and (iii) show three different excitation ways for electrons moving to the trap center through the CB. The quantum tunnelling (QT) effect is another possible path for electron trapping. (a-c) Reprinted (adapted) with permission from Ref. 132. Copyright (2014) American Chemical Society. (d) Reproduced from ref. 133 with permission from The Royal Society of Chemistry.

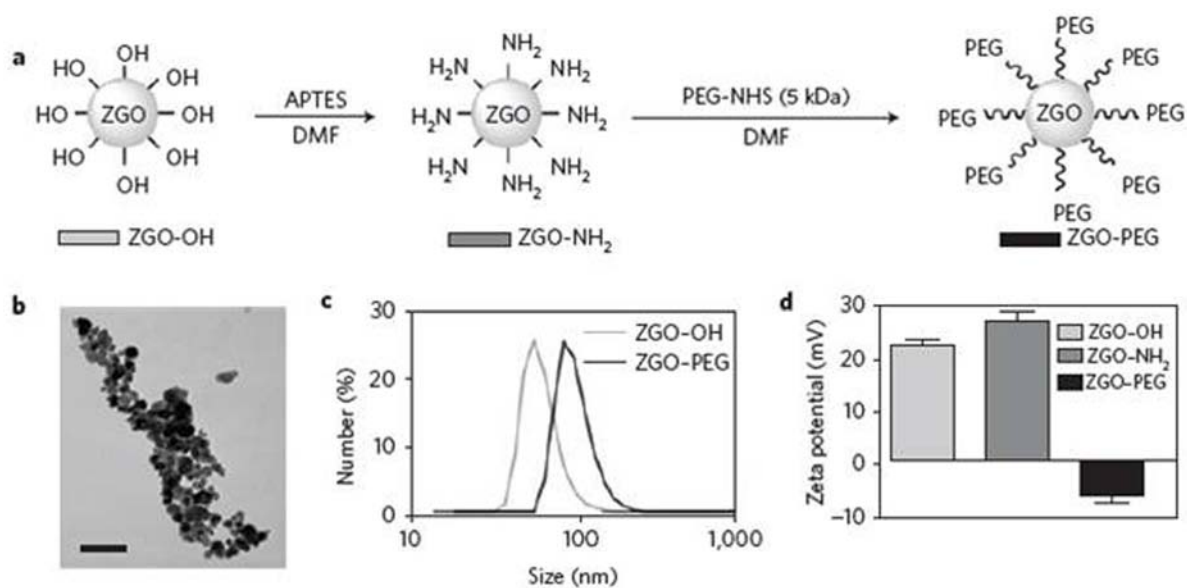


**Fig. 9** The surface functionalization and characterization of red-excitable PLNPs. **(a)** A schematic representation of ZGO-OH surface functionalization; **(b)** A transmission electron micrograph of ZGO-OH nanoparticles. Scale bar, 100 nm; **(c)** The hydrodynamic diameter measured by dynamic light scattering in 5% glucose before and after PEG coverage; **(d)** The evolution of zeta potential as a function of surface coverage. Reprinted by permission from Macmillan Publishers Ltd: [Nature material] (Ref 134), copyright (2014)

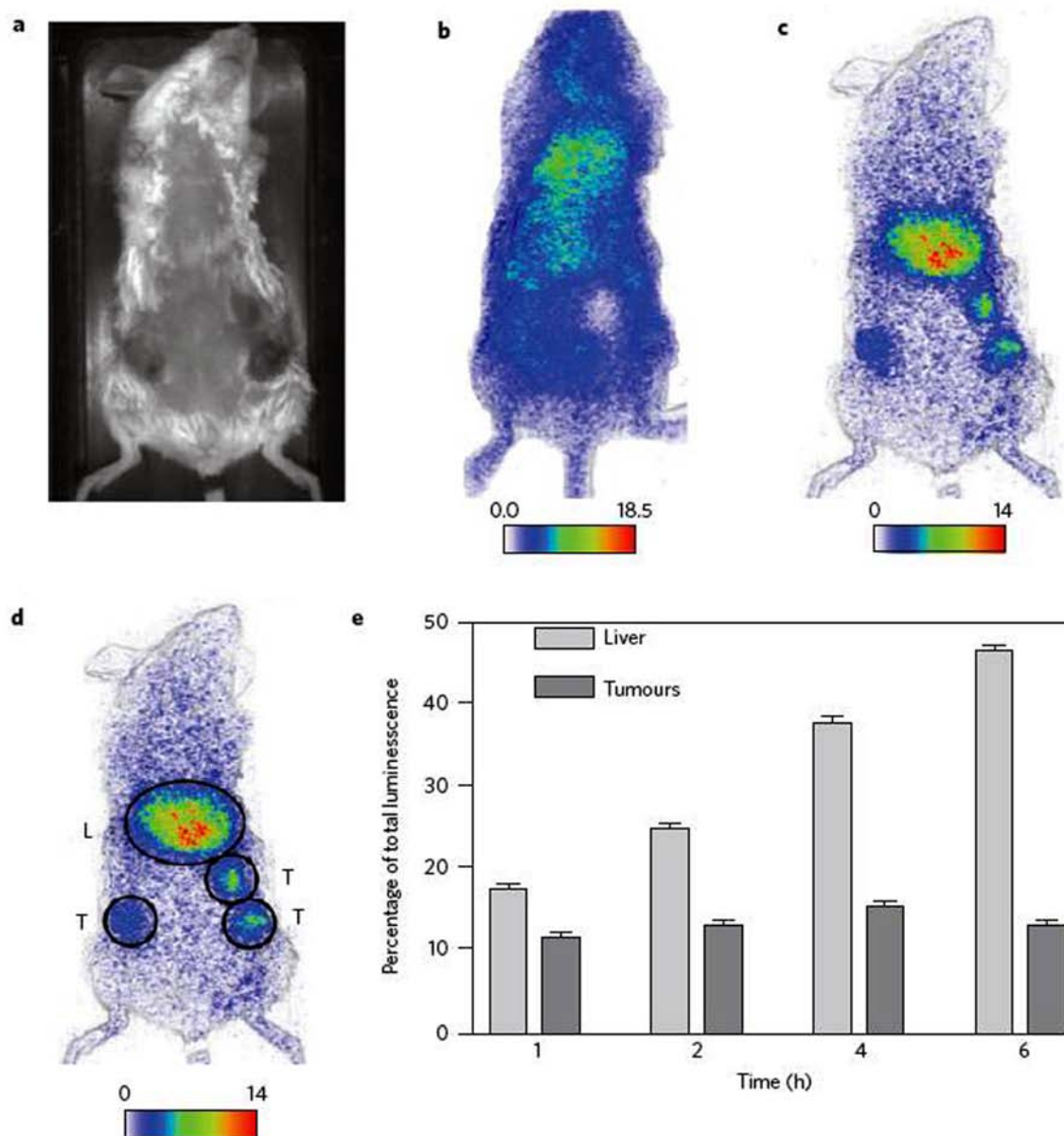


**Fig. 10** The biodistribution of stealth ZGO-PEG nanoparticles in tumour-bearing mice ( $n=3$ ), (a) Optical image of a tumour-bearing mouse; (b) Persistent luminescence image of a tumour-bearing mouse, 2 h after the injection of ZGO-PEG nanoparticles excited by an ultraviolet lamp for 2 min (acquisition time: 10 min); (c) Persistent luminescence image of a tumour-bearing mouse immediately after LED illumination, 4 h after the injection of ZGO-PEG nanoparticles excited by an ultraviolet lamp for 2 min (acquisition time: 3 min); (d) Schematic ROI drawn for semi-quantization analysis- L-liver, T-tumour; (e) Semi-quantization of the accumulation kinetics in the main labelled tissues expressed as a percentage of the total luminescence detected from the whole animal. Persistent luminescence intensity is expressed in false colour units (1 unit D 2,800 photons  $s^{-1}.cm^2.sr$ ) in all images. Reprinted by permission from Macmillan Publishers Ltd: [Nature material] (Ref 134), copyright (2014)

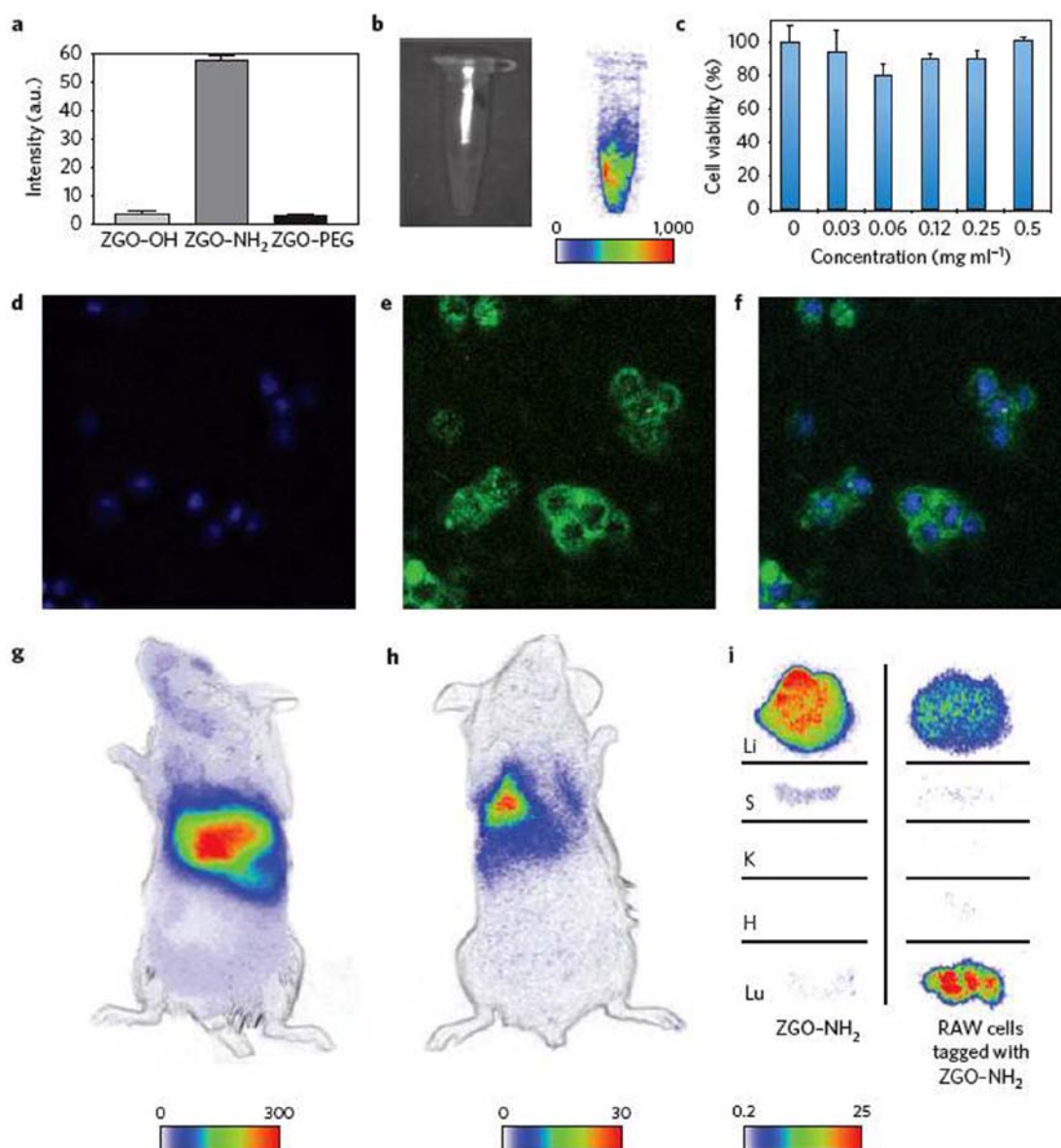


**Fig. 11** Cellular tracking with persistent luminescence after LED excitation. (a) Phagocytosis efficiency expressed as persistent luminescence signal retained by RAW macrophages that have incorporated differently charged ZGO nanoparticles; (b) Optical and persistent luminescence image of tagged RAW cells suspended in culture medium (3 min acquisition time); (c) *In vitro* cellular toxicity of ZGO-NH<sub>2</sub> nanoparticles towards RAW cells (MTT, 3-(4,5-dimethyl-2-thiazolyl)-2,5-diphenyltetrazolium bromide, assay). Nanoparticles were incubated with cells for 6 h; (d) Confocal microscopy image of TOPRO staining (blue) on tagged RAW cells; (e) Confocal microscopy image of FITC-grafted ZGO nanoparticles (green), taken up by RAW cells; (f) Merged confocal microscopy image of RAW cells stained with both TOPRO and FITC-grafted PLNPs; (g) Biodistribution of ZGO-NH<sub>2</sub> nanoparticles in healthy mouse, 15 min after systemic injection (acquisition time: 1 min); (h) Biodistribution of RAW cells tagged with ZGO-NH<sub>2</sub> nanoparticles in healthy mouse, 15 min after systemic injection (acquisition time: 1 min); (i) *Ex vivo* biodistribution of free ZGO-NH<sub>2</sub> and RAW macrophages tagged with ZGO-NH<sub>2</sub> nanoparticles 24 h after intravenous injection, Li-liver, S-spleen, K-kidneys, H-heart, Lu-lungs. Persistent luminescence intensity is expressed in false colour units (1 unit D 2,800 photons s<sup>-1</sup>.cm<sup>2</sup>.sr) for all images. Reprinted by permission from Macmillan Publishers Ltd: [Nature material] (Ref 134), copyright (2014)

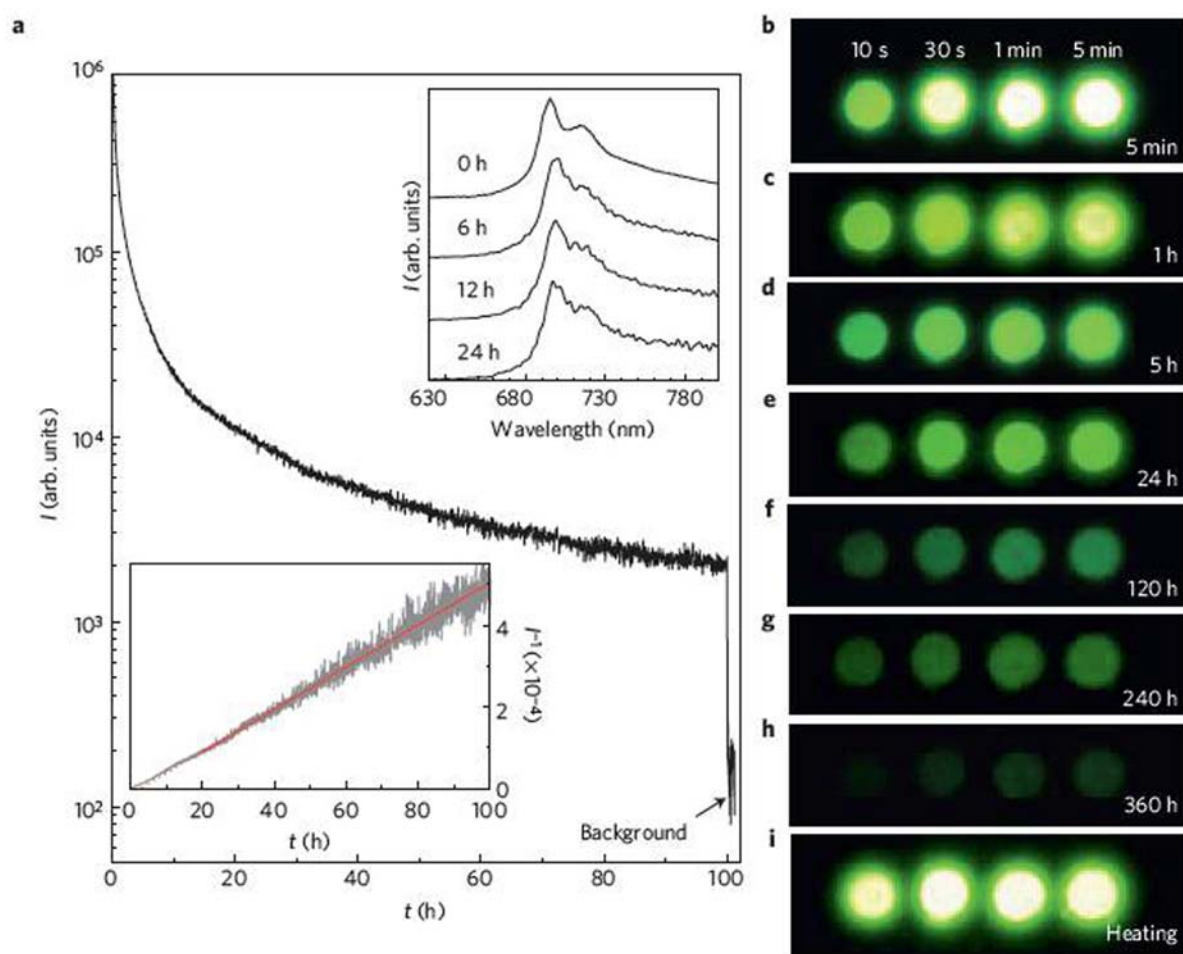


**Fig. 12** NIR afterglow decay of  $\text{Zn}_3\text{Ga}_2\text{Ge}_2\text{O}_{10}: 0:5\%\text{Cr}^{3+}$  discs irradiated by a 4 W 365 nm ultraviolet lamp. **(a)** Afterglow intensity ( $I$ ) monitored at 713 nm as a function of time ( $t$ ). The sample was irradiated for 5 min. The bottom inset shows the same data plotted as  $I^{-1}$  versus  $t$ . The upper inset shows four afterglow spectra recorded at 0 h, 6 h, 12 h and 24 h after the stoppage of the irradiation; **(b–h)** NIR images of four phosphor discs taken at different afterglow times (5 min to 360 h) after irradiation by a 365 nm lamp for 10 s to 5 min. The discs were placed on a hot plate surface for imaging. Imaging parameters: **b–d**, auto/ISO 200/0.3–4 s; **e**, manual/ISO 200/30 s; **f–h**, manual/ISO 400/30 s. **i**, NIR image of the four 360-h-decayed discs when heated at  $\sim 400^\circ\text{C}$  on the hot plate. Imaging parameters: auto/ISO 200/0.3 s. Reprinted by permission from Macmillan Publishers Ltd: [Nature material] (Ref 137), copyright (2012)

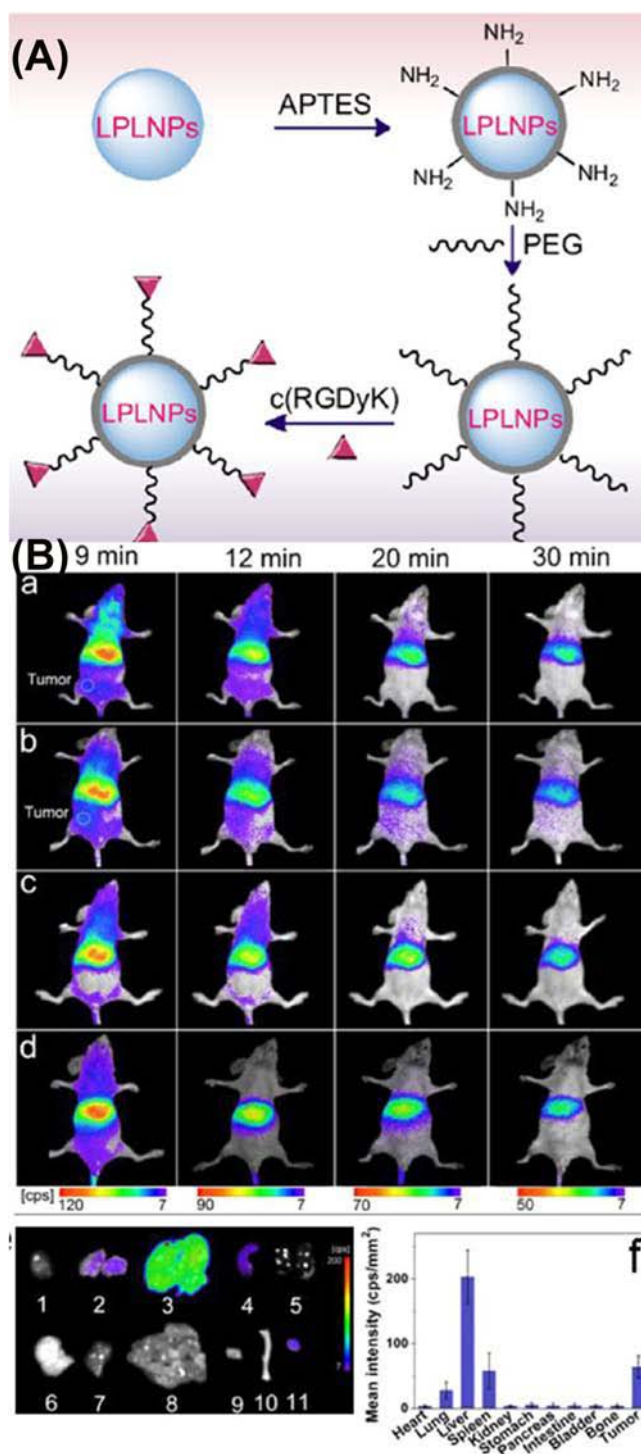


**Fig. 13** (A) Schematic illustration for the surface modification of the LPLNPs; (B)-In vivo NIR luminescence images of U87MG tumour-bearing mice (white circles locate the tumour site): (a, b) and normal mice, (c, d) after intravenous injection of PEG-LPLNPs (a, c) and RGD-LPLNPs (b, d) (0.4 mg, 10 min irradiation with a 254 nm UV lamp before injection). (e) Representative *ex vivo* NIR luminescence images of isolated organs and tumour from a U87MG tumour-bearing mouse at 6 h post-intravenous injection of RGD-LPLNPs (0.4 mg): (1) heart, (2) lung, (3) liver, (4) spleen, (5) kidney, (6) stomach, (7) pancreas, (8) intestine, (9) bladder, (10) bone, (11) tumour. (f) Semi-quantification of RGD-LPLNPs in the isolated organs and tumour of the mice, error bars represent one standard deviation of triplicate

measurements from individual animals. Reprinted (adapted) with permission from Ref. 138. Copyright (2013) American Chemical Society.

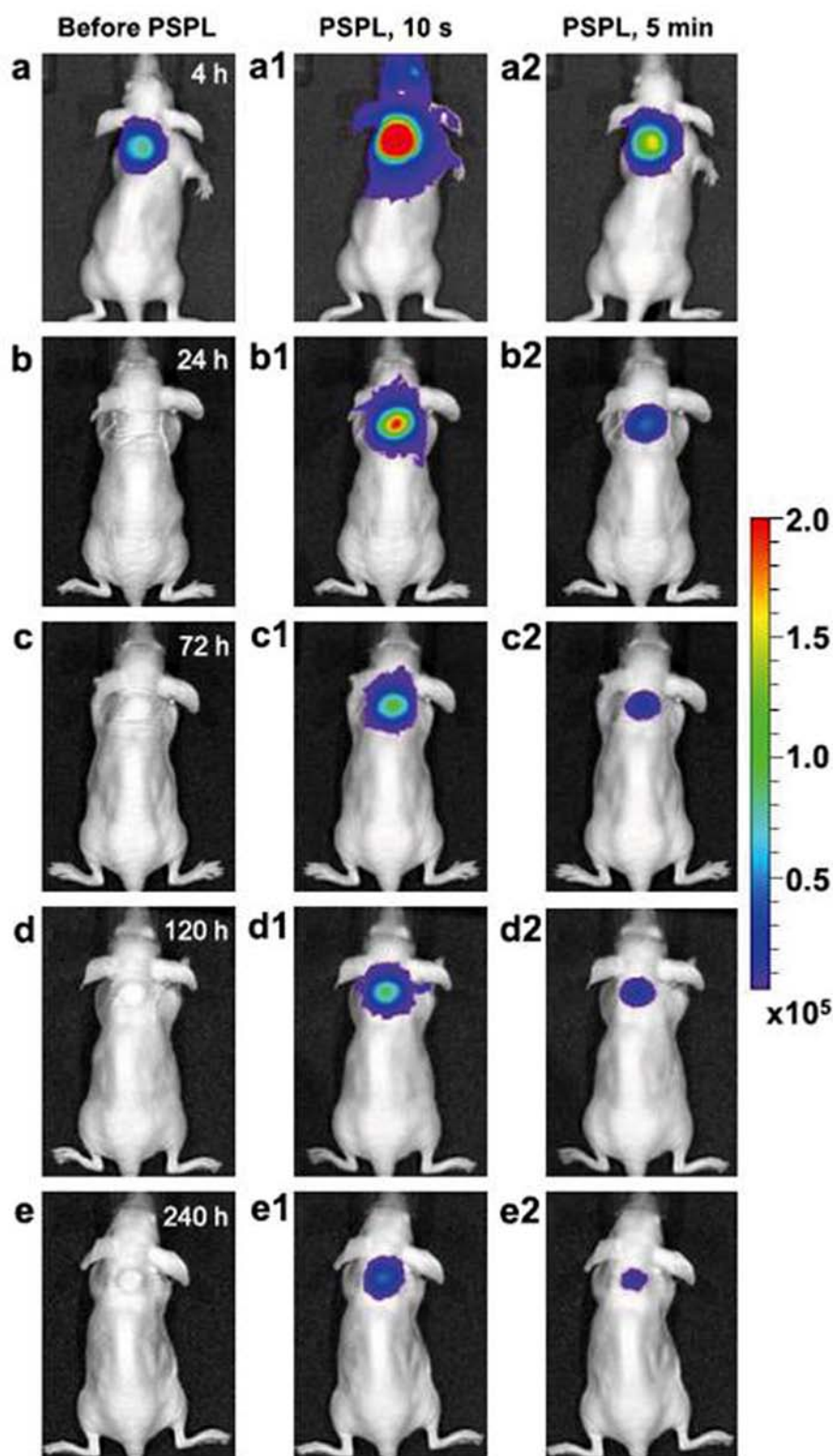


**Fig. 14** Images of PEI-LiGa<sub>5</sub>O<sub>8</sub>:Cr<sup>3+</sup> nanoparticles labeled 4T1 cells injected into a nude mouse for a 10-day tracking using an IVIS imaging system. The PEI-LiGa<sub>5</sub>O<sub>8</sub>:Cr<sup>3+</sup>

nanoparticles labeled 4T1 cells ( $\sim 2.5 \times 10^7$  cells) were illuminated by a 4 W 254 nm UV lamp for 15 min, and then subcutaneously injected into the back of a nude mouse. **(a)** Image taken at 4 h after cell injection. To get the PSPL signal, the mouse was exposed to a white LED flashlight (Olight SR51, 900 lumens) for 15 s. **(a1)** and **(a2)**, Images taken at 10 s and 5 min after the stimulation, respectively. The signals were attributed to PSPL. **(b-e)** The mouse was exposed daily to the LED flashlight for 15 s, and images were taken at 10 s and 5 min after the stimulation. All images were acquired in the bioluminescence mode with an exposure time of 2 min. The images were processed using Living Image software at binning of 4 and smooth of 535. The color scale bar represents the luminescence intensity in the unit of radiance,  $\text{p/sec/cm}^2/\text{sr}$ . Reprinted by permission from Macmillan Publishers Ltd: [Scientific Reports] (Ref 141), copyright (2013).

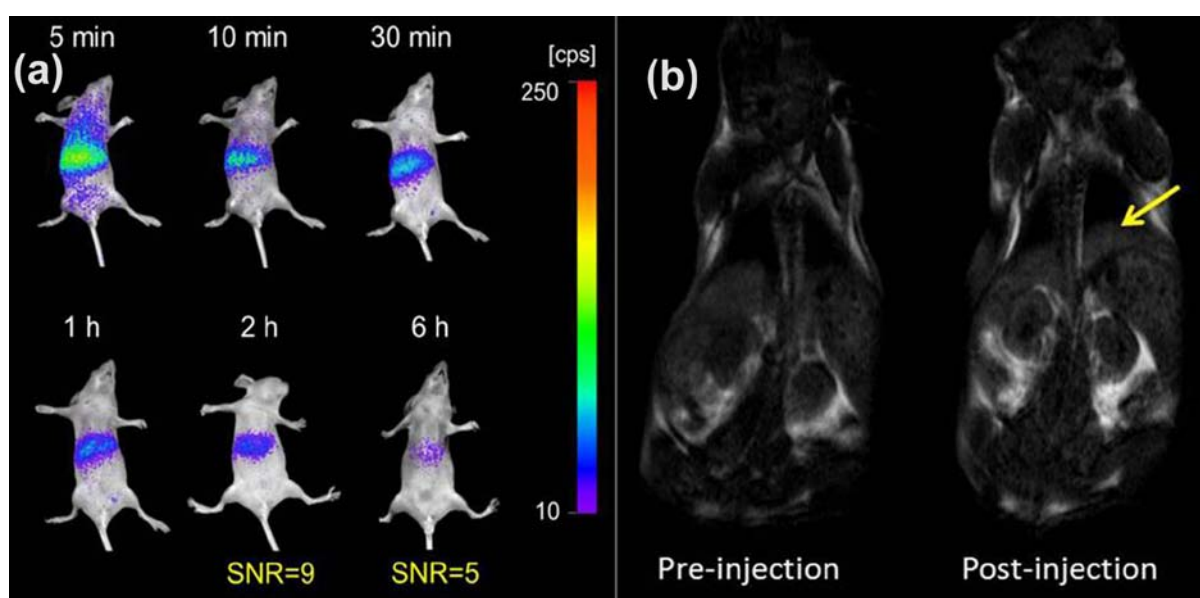
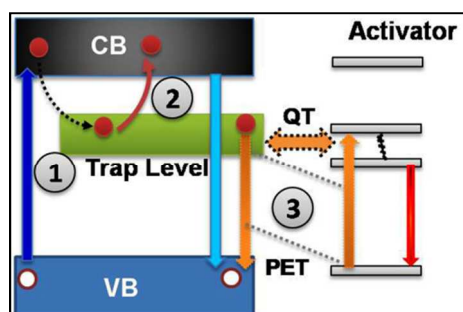


**Fig. 15** **(a)** *In vivo* NIR luminescence images of a normal mouse after intravenous injection of Gd(III)-PLNPs (0.3 mg, 10 min irradiation with a 254 nm UV lamp before injection but without irradiation during imaging); **(b)** *In vivo* T<sub>1</sub>-weighted MR images of the mouse before and after intravenous injection of Gd(III)-PLNPs (0.3 mg); the yellow arrow indicates the liver. Reprinted (adapted) with permission from Ref. 51. Copyright (2014) American Chemical Society.



**Sunil K Singh**, born in 1982, received doctoral degree in Physics in 2011 from the Banaras Hindu University, India. Currently, he is a DST-INSPIRE faculty at Indian Institute of Technology (Banaras Hindu University), Varansi, India. His research interest includes Physics of multimodal luminescence (upconversion, downconversion/quantum-cutting, downshifting) including persistent luminescence in lanthanide doped nanostructures. In terms of applications, the focus is on bio-imaging, to increase the conversion efficiency of photovoltaic cells, sensors, and for security purposes, *etc.* He has authored/co-authored a book chapter, a review article and more than 30 peer-reviewed journal articles, and his current h-index is 11 (Sep. 2014).

## Table of Contents



Schematic representation of different process in persistent luminescence: charging (1), stimulation (2), discharging (3) (PET-persistent energy transfer, QT-quantum tunneling).